Journal of Marine Research, 56, 197–238, 1998

Simulation of primary production and export fluxes in the Northwestern Mediterranean Sea

by Marina Lévy[1], Laurent Mémery[1] and Jean-Michel André[2]

ABSTRACT

A biogeochemical model, BIOMELL (BIOgeochemical Model of the Euphotic Layer of Lodyc), has been developed to simulate the temporal evolution of the main nitrogen stocks and fluxes at the DyFAMed station (Dynamique des Flux Atmospheriques en Mediterranée), located in the Northwestern Mediterranean Sea. This mainly oligotrophic region is characterized by a strong seasonal cycle, and a significant export of dissolved organic matter compared to the particulate export measured by sediment traps. Validation of the model is made using temperature, nitrate and chlorophyll profiles acquired at DyFAMed approximately every month in 1991. Extended datasets from specific years are also used to validate seasonal variations of other variables, for which the coverage in 1991 was rather poor (new and total production, particulate export, dissolved organic matter export, bacteria, zooplankton). Sensitivity studies on selected parameters are carried out in order to give an idea of the margin of error in the model predictions. The model is then used to analyze the behavior of the biogeochemical system during various production regimes (winter, spring bloom, oligotrophy, autumn bloom). It is shown that several processes, which are often neglected in biogeochemical models, must be taken into account: phytoplankton growth limitation by deep mixing, C:Chl ratio dependence on light, nitrification, and semi-refractory dissolved organic matter accumulation in the surface layer.

1. Introduction

The role of the ocean as regards carbon dioxide assimilation is a key question concerning climatic and environmental changes (Houghton *et al.,* 1990; Siegenthaler and Sarmiento, 1993). Within the ocean, primary production and export fluxes are the biological processes that ought to be understood and evaluated. As a matter of fact, together with oceanic dynamics, they control total inorganic carbon content of the mixed layer, which is directly in contact with the atmosphere, and thus the carbon dioxide exchange between the ocean and the atmosphere (Longhurst and Harrison, 1989).

Due to seasonal and regional variations of the climatic forcings and oceanic dynamics, various specific regimes of primary production take place in the world ocean; for instance the oligotrophic subtropical gyre systems, the upwelling areas, the large-scale spring

1. LODYC, Université Pierre et Marie Curie, 5 Place Jussieu, 75252 Paris Cedex 05, France.
2. ORSTOM, Centre de Noumea, Noumea Cedex, New Caledonia.

blooms or the winter regime in convective regions. In order to build realistic dynamical-biological coupled models of the world ocean, each regime must be understood. In this respect, the Mediterranean Sea can be considered as an interesting target as several of these regimes can be found in a rather small area. In particular, in the northern basin, deep convection occurs during winter, leading to a spring bloom. Oligotrophy prevails during summer while perturbations in the meteorological forcing generate a secondary bloom in fall. Another reason for dedicating a study to the Mediterranean Sea is that it is relatively well known. More specifically, the Dynamique des Flux Atmospheriques en Mediterranée (DyFAMed) program, part of the France-Joint Global Ocean Flux Study (France-JGOFS), provides a rich dataset of biological, geochemical, and physical parameters, which allowed us to carry out and validate simulations (Marty, 1993).

The aim of the present work is to achieve a 1D modeling study throughout the annual cycle in the Northwestern Mediterranean Sea, paying particular attention to physical controls on primary production and export fluxes. Several biogeochemical models of the carbon, nutrients and plankton cycles have already been published (Fasham *et al.,* 1990, hereafter FDM; McGillicuddy *et al.,* 1995), but failed in predicting correct export fluxes. The present modeling relies essentially on these models, with an improved description of particulate and dissolved matter fluxes exported from the surface layer.

First we present a brief description of the dynamics in the Northwestern Mediterranean and of the main features concerning primary productivity, based on recent *in situ* measurements. Then a detailed description of the BIOgeochemical Model of the Euphotic Layer of Lodyc (BIOMELL) is provided. Finally we simulate an annual cycle at the DyFAMed station and perform model sensitivity studies. The behavior of the model during the various production regimes is validated and analyzed.

2. Present knowledge

a. The hydrological and productivity characteristics of the region

The DyFAMed station is located 52 km southeast of Nice, at 43°25N, 07°52E (Fig. 1). 2350 m deep, it is in the central zone of the Ligurian Sea, the northeastern part of the Western Mediterranean Sea, bounded by the French (Provence, Corsica) and Italian (Gulf of Geneva) coasts. The circulation of the Ligurian Sea is characterized by a permanent cyclonic gyre (Millot, 1987). The Ligurian Current flows along the coast inside a strip about 30 km wide. It is separated from the offshore central zone by a frontal zone identified by a rapid horizontal change of density. The DyFAMed station is far enough away from the Ligurian Current to be sufficiently protected from lateral transport and to justify a 1D study (Marty, 1993). The density structure of the zone has the shape of a dome, with minimal stratification at the center. In winter, a succession of strong and dry continental wind events occurs over the gyre. The surface stratification is progressively eroded in the vortex center. Intense vertical convection occurs within the central zone, mixing the cool dense surface water and the underlying saltier Levantine intermediate water. This mixing results in local

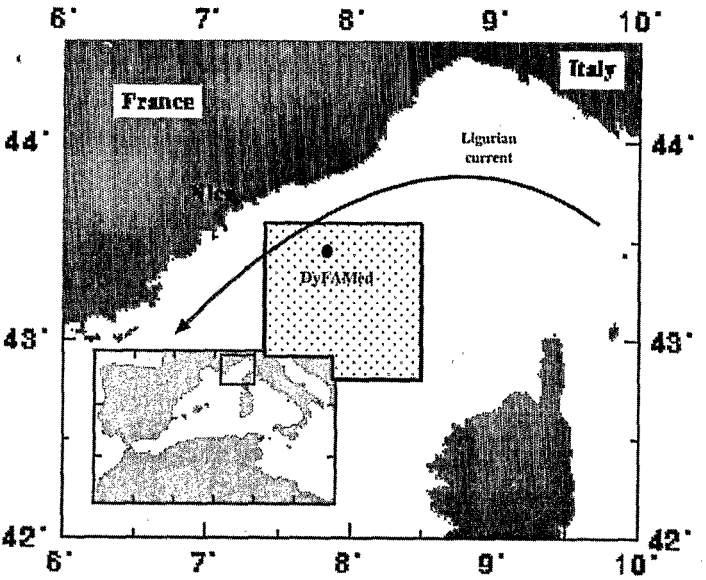

Figure 1. Location of the DyFAMed station. This station is located outside the coastal Ligurian current, and is typical of the offshore Northwestern Mediterranean Sea. The main cyclonic circulation is shown by arrows. The area over which ECMWF atmospheric model heat flux and wind data have been extracted for the use of this study is shown by the speckled square.

deep water formation typical of the western basin (Medoc group, 1970). This process, achieved through baroclinic instabilities (Gascard, 1978), emphasizes the limits of the one-dimensional behavior of the water column physics at DyFAMed.

The winter mixing also brings nutrients into the upper layer. However, the short residence time of algae in this layer, swept along by the vertical water motions, prevents the development of biomass (hereafter referred as "deep-mixing limitation" process, André, 1990). Short periods of stabilization during winter (due to good weather conditions) can occur and are associated with short-lived diatom blooms (DyFAMed, 1995). Progressing in the year, the surface layer becomes stable over a longer period, thus allowing the winter nutrient enrichment to be utilized continuously. As a consequence, algae are blooming. From Coastal Zone Color Scanner (CZCS) observations, Morel and André (1991) have observed this change of regime, between early April and mid-May. After mid-May and until November, the situation remains steady. The upper layer nutrient content is very low, the system is mainly oligotrophic and characterized by a deep chlorophyll maximum (DCM) (Jacques *et al.*, 1976). As the heat budget becomes negative in late autumn, the thermocline begins to erode, which brings nutrients again into the upper layer and allows a secondary bloom to occur. This autumnal bloom is less extended than the spring bloom, with lower surface pigment concentrations (Morel and André, 1991).

b. Primary production and export fluxes in the Northwestern Mediterranean Sea

Primary or total production (TP) can be partitioned into new production (NP), supplied by vertical transports of nutrients from below the euphotic layer, and into regenerated production (RP), based on nutrients recycled within the productive layer. Following Dugdale and Goering (1967), NP is associated with nitrate assimilation, while RP is linked to ammonium uptake. However, recent measurements in surface waters of the Mediterranean Sea show significant nitrification rates, which can be a source of locally recycled nitrate, implying that nitrate utilization cannot be simply associated with NP (Gentilhomme, 1992; Ward, 1986; Ward *et al.*, 1989). Evidence of apparent nitrification in the first hundred meters of the water column have also been reported in Eppley *et al.* (1990) and in Eppley and Koeve (1990). In the North Mediterranean Basin, TP is about 80 $gCm^{-2}y^{-1}$ (Minas, 1970). Based on phosphate or oxygen balance, NP estimates are 12–35 $gCm^{-2}y^{-1}$ (Bethoux, 1989). Nitrification measurements in the Almeria-Oran frontal system (Bianchi *et al.*, 1993) shows that nitrification may supply 40% of the nitrate assimilation in the euphotic layer.

At steady state, the rate of new nitrogen assimilation (nitrate assimilation minus nitrification) must equal the rate of nitrate supply, and must be balanced by export. It has long been believed that this export is achieved largely by sinking particles (Eppley and Peterson, 1979). The mean value of vertical flux of particulate organic carbon at 200 m for 1987–1990, estimated from sediment traps, is 4 $gCm^{-2}\ y^{-1}$ (Miquel *et al.*, 1994). But new observations of the dissolved organic carbon (DOC) annual cycle show that the export of DOC can equal or exceed the particle export caught in traps (Carlson *et al.*, 1994). Estimated DOC export (from DOC contents) is 14.8 $gCm^{-2}\ y^{-1}$ in the Mediterranean Sea (Copin-Montegut and Avril, 1993). This large DOC export flux reconciles organic carbon flux estimates with NP data (Marty *et al.*, 1994a).

3. The BIOMELL

a. General presentation

Most biogeochemical models follow the general structure of the FDM model (Drange, 1994; Prunet *et al.*, 1996). They consist of different compartments describing nitrate, ammonium, phytoplankton, zooplankton, bacteria, detritus, and dissolved organic matter (DOM), and use nitrogen as currency. Interactions among these compartments are designed to represent the main biogeochemical processes. BIOMELL is in the line of these models, and has been developed more specifically to represent adequately the processes involved in primary production and export fluxes, that are believed to be important in the Mediterranean Sea, such as DOM export, nitrification and deep-mixing limitation, and that were not treated in FDM. To better represent the export of organic carbon from the surface waters, the compartments involved in the export; i.e. dissolved and particulate organic matter, have been reformulated. As a result, each organic matter compartment (particulate and dissolved) is divided into two subcompartments. The particulate compartment is divided into small and large detritus subcompartments, and the DOM compartment is

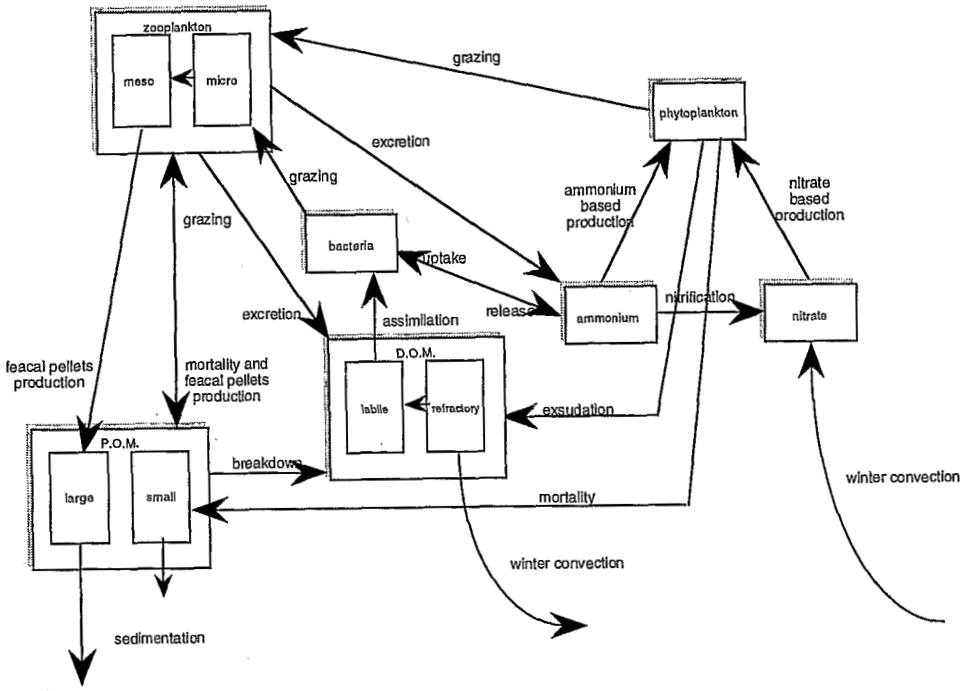

Figure 2. Schematic representation of the compartments and processes of the BIOMELL.

divided into refractory DOM and labile DOM. The small detritus and the labile DOM concern mostly regeneration. The large detritus, comparable to the matter measured in sediment traps, and the refractory DOM that accumulates in the mixed layer until the winter destratification, represent the basic pools implied in export fluxes.

b. The biogeochemical processes and the associated equations

A schematic representation of the compartments and processes involved in BIOMELL is shown Figure 2 (corresponding equations are given Table 1). All biogeochemical concentrations are submitted to vertical mixing.

i. Nutrients (Eq. 1–2). In order to discriminate between new and regenerated production (Dugdale and Goering, 1967), the model deals with two nutrients: nitrate as supporting NP (as far as local nitrification does not occur) and ammonium as supporting RP. Nitrate is mainly supplied to the productive layer by winter convection (through mixing processes) but also by nitrification. At steady state, these supplies are balanced by phytoplankton uptake. Ammonium is produced by bacteria mortality and zooplankton excretion. It is uptaken by phytoplankton and bacteria. It contributes to nitrate production by nitrification. Dependent nitrate and ammonium uptakes are parameterized according to Hurtt and Armstrong (1996). This parameterization uses only one parameter (half-saturation constant

Table 1. Equations 1 to 10 describe the temporal partial derivatives of respectively nitrate (NO_3), ammonium (NH_4), phytoplankton (P), microzooplankton (Z_s), mesozooplankton (Z_l), bacteria (B), small detritus (D_s), large detritus (D_l), labile dissolved organic matter (DOM_l), and refractory dissolved organic matter (DOM_r). The first term on the right-hand side of these equations accounts for vertical mixing (k_z being the vertical diffusion coefficient). The other terms are the biogeochemical sink/source terms that distribute nitrogen between compartments. Eqs. 11 to 16 describe the computation of the Carbon:Chlorophyll ratio. Eqs. 17 to 27 define the notations that are being used in equations 1 to 10 (except for the parameters that are defined Table 2).

$$\partial_t NO_3 = \partial_z(k_z\partial_z NO_3) - JL_{no_3}L_M P + R_{nh_4}L_T NH_4 \tag{1}$$

$$\partial_t NH_4 = \partial_z(k_z\partial_z NH_4) - JL_{nh_4}L_M P - U^{nh4} - R_{nh_4}L_T NH_4 + \epsilon_{z_l}\mu_{z_l}Z_l + \epsilon_{z_s}\mu_{z_s}Z_s + m_b B + \eta G^b_{z_s} R^{bac}_{c:n}/R^{phy}_{c:n} \tag{2}$$

$$\partial_t P = \partial_z(k_z\partial_z P) + (1-\gamma)J(L_{no_3} + L_{nh_4})L_M P - G^p_{z_s} - G^p_{z_l} - m_p P \tag{3}$$

$$\partial_t Z_s = \partial_z(k_z\partial_z Z_s) + a^p_{z_s}G^p_{z_s} + (a^b_{z_s} - \eta R^{bac}_{c:n}/R^{phy}_{c:n})G^b_{z_s} + a^{d_s}_{z_s}G^{d_s}_{z_s} - \mu_{z_s}Z_s - m_{z_s}Z_s - G^{z_s}_{z_l} \tag{4}$$

$$\partial_t Z_l = \partial_z(k_z\partial_z Z_l) + a^p_{z_l}G^p_{z_l} + a^{z_s}_{z_l}G^{z_s}_{z_l} + a^{d_s}_{z_l}G^{d_s}_{z_l} - \mu_{z_l}Z_l - m_{z_l}Z_l \tag{5}$$

$$\partial_t B = \partial_z(k_z\partial_z B) + U^{nh_4} + U^{dom_l} - m_b B - G^b_{z_s} \tag{6}$$

$$\partial_t D_s = \partial_z(k_z\partial_z D_s) + (1-a^p_{z_s})G^p_{z_s} + (1-a^b_{z_s})G^b_{z_s} + (1-a^{d_s}_{z_s})G^{d_s}_{z_s} + m_p P + m_{z_s}Z_s + m_{z_l}Z_l - \mu_{d_s}D_s - G^{d_s}_{z_l} - G^{d_s}_{z_s} - V_{d_s}\partial_z D_s \tag{7}$$

$$\partial_t D_l = \partial_z(k_z\partial_z D_l) + (1-a^{z_s}_{z_l})G^{z_s}_{z_l} + (1-a^p_{z_l})G^{p_s}_{z_l} + (1-a^{d_s}_{z_l})G^{d_s}_{z_l} - \mu_{d_l}D_l - V_{d_l}\partial_z D_l \tag{8}$$

$$\partial_t DOM_l = \partial_z(k_z\partial_z DOM_l) + (1-\epsilon_{z_l})f_{dom_l}\mu_{z_l}Z_l + (1-\epsilon_{z_s})f_{dom_l}\mu_{z_s}Z_s + f_{dom_l}\gamma J(L_{no_3} + L_{nh_4})L_M P + f_{dom_l}\mu_{d_s}D_s + f_{dom_l}\mu_{d_l}D_l + \mu_{dom_r}DOM_r - U^{dom_l} \tag{9}$$

$$\partial_t DOM_r = \partial_z(k_z\partial_z DOM_r) + (1-\epsilon_{z_l})(1-f_{dom_l})\mu_{z_l}Z_l - \mu_{dom_r}DOM_r + (1-\epsilon_{z_s})(1-f_{dom_l})\mu_{z_s}Z_s + (1-f_{dom_l})\gamma J(t,z)(L_{no_3} + L_{nh_4})L_M P + (1-f_{dom_l})\mu_{d_s}D_s + (1-f_{dom_l})\mu_{d_l}D_l \tag{10}$$

minimal Chlorophyll:Nitrogen ratio
$$R^{\min}_{chl:n} = 12R^{phy}_{c:n}/R^{\max}_{c:chl} \tag{11}$$

maximal Chlorophyll:Nitrogen ratio
$$R^{\max}_{chl:n} = 12R^{phy}_{c:n}/R^{\min}_{c:chl} \tag{12}$$

optimal Chlorophyll:Nitrogen ratio when $PUR > PUR_{\max}$
$$R^{*}_{chl:n} = R^{\min}_{chl:n}$$
$$R^{*}_{chl:n} = \left(R^{\max}_{chl:n} - (R^{\max}_{chl:n} - R^{\min}_{chl:n})\frac{PUR}{PUR_{\max}}\right) \tag{13}$$

Table 1. (Continued)

optimal Chlorophyll:Nitrogen ratio when $PUR < PUR_{\max}$	$\cdot \dfrac{NO_3 + NH_4}{K_{nh_4} + NO_3 + NH_4}$	(14)
Chlorophyll:Nitrogen ratio	$\partial_t R_{chl:n} = \dfrac{(R_{chl:n} - R^*_{chl:n})}{J(L_{no_3} + L_{nh_4})L_M}$	(15)
Carbon:Chlorophyll ratio	$R_{c:chl} = 12R^{phy}_{c:n}/R_{chl:n}$	(16)
nitrate limitation on phytoplankton growth	$L_{no_3} = \dfrac{K_{nh_4}NO_3}{(K_{nh_4} + NH_4)(K_{nh_4} + NO_3 + NH_4)}$	(17)
ammonium limitation on phytoplankton growth	$L_{nh_4} = \dfrac{NH_4}{NH_4 + K_{nh_4}}$	(18)
temperature limitation on phytoplankton growth	$L_T = a_T{}^{(T-T^{opt})}$	(19)
deep mixing limitation on phytoplankton growth	L_M depends on mixed layer and euphotic layer depths (see text for more details)	(20)
light dependent phytoplankton growth	$J = 12/R_{c\text{-}chl}\, a^*_{\max}\psi_{\mu\max} \times KPUR^{opt} \times L_T \times (1 - e^{-PUR/KPUR^{opt}\times L_T}) \times e^{-\beta\times PUR/KPUR^{opt}\times L_T}$	(21)
grazing ($Y = P, B, Z_s$ or D_s and $X = Z_s$ or Z_l)	$G^Y_X + g_X f_T X \dfrac{p^Y_X Y}{K_X + F_X}$	(22)
preferences ($Y = P, B, Z_s$ or D_s and $X = Z_s$ or Z_l)	$p^Y_X = \dfrac{\check{p}^Y_X}{\sum_Y \check{p}^Y_X Y}$	(23)
total food availability ($Y = P, B, Z_s$ or D_s and $X = Z_s$ or Z_l)	$F_X = \sum_Y p^Y_X Y$	(24)
temperature limitation on zooplankton grazing	$f_T = \left(\dfrac{T_{\max} - T}{T_{\max} - T_{opt}}\right)^{(T_{\max}-T_{opt})/R_g} \exp\left(\dfrac{T - T_{opt}}{R_g}\right)$	(25)
substrate for bacteria	$S = \min(NH_4, \eta DOM_l)$	(26)
ammonium bacterial uptake	$U^{nh_4} = L_T V_b B \dfrac{S}{K_b + S(1 + 1/\eta)}$	(27)
labile DOM bacterial uptake	$U^{dom_l} = L_T V_b B \dfrac{S/\eta}{K_b + S(1 + 1/\eta)}$	(28)

for ammonium) compared to three in the more classical representation by FDM (half-saturation constant for nitrate and for ammonium and ammonium inhibition parameter), and keeps the inhibition effect of ammonium on nitrate uptake, meaning that phytoplankton preferentially takes up ammonium (Eq. 17–18), in agreement with data (Harrison *et al.*, 1996).

ii. Phytoplankton, (Eq. 3). A unique generic phytoplankton compartment is considered. This can be a limitation when dealing with the spring succession from large, fast sinking diatoms to small, slowly sinking cells (Raimbault *et al.*, 1988). Nitrogen exudation as DOM is assumed to be a constant fraction of total net primary production. The other phytoplankton loss terms are grazing by zooplankton and natural mortality. Mortality is defined by a constant rate, and fuels the small detritus compartment.

The photosynthetic growth rate (in carbon unit per chlorophyll unit) is modeled according to Morel (1991) (Eq. 19–21), as a function of the Photosynthetic Usable Radiation (PUR), computed from the Photosynthetic Available Radiation (PAR) using a mean absorption spectrum. The PAR is predicted as a function of phytoplankton pigment content according to the spectral algorithm of Morel (1988). The growth rate is converted to s^{-1} using time dependent C:Chl ratios (Eq. 21). Following Doney *et al.* (1996), the C:Chl ratio is driven by irradiance and nutrient concentrations. In BIOMELL, this ratio is damped toward a local C:Chl value, which varies with the mean PUR of the previous day's sunlight hours. The time constant of this damping is given by the growth time of phytoplankton (Eq. 15–16), which is considered as the adaptation time of the planktonic biomass. Its order of magnitude is equal to about one day. Above a threshold value of the PUR (PUR_{max}), this parameter is set to its maximum value $R_{C:Chlmax}$ (Eq. 11–13). Below that level, the C:Chl ratio decreases with PUR, bounded by a lower value $R_{C:Chlmin}$ (Eq. 11–12–14).

The inhibition of primary production when the mixed layer is significantly deeper than the euphotic layer has been observed earlier (Gran and Braarud, 1935; Riley, 1942). Sverdrup's (1953) model gave the first statements allowing the growth of an algal population to be diagnosed as a function of the mixed layer depth to the compensation depth ratio. Previous studies (Woods and Onken, 1982; Yamazaki and Kamykowski, 1991) used a Lagrangian approach to model cell trajectories in the light gradient and gave some quantitative insight on the biological response to deep vertical mixing. Their results, however, do not provide a simple representation for prediction of growth rates as a function of photosynthetic capacity and of vertical mixing intensity during winter. Such a simple parameterization can be developed on the basis of André's (1990) study of the Northwestern Mediterranean winter regime. His work assumes that only the fraction of the population that spends enough time in the euphotic layer to insure cell division contributes to the global growth, the rest being swept away into the dark part of the mixed layer where respiration prevails. In the frame of 1D vertical homogeneous turbulent diffusion, an ensemble Lagrangian approach allowed this fraction (L_M) to be computed as a function of

the vertical diffusion coefficient (k_z) for typical values of doubling time and euphotic layer depth (Z_E), when the mixed-layer depth (Z_M) is significantly deeper ($Z_M > 2Z_E$). With doubling times of 1–2 days, Z_E in the range of 50 to 100 m and k_z of 10^{-3} to 10^{-1} m^2 s^{-1}, L_M varies between 0 and 30%. In order to integrate these results in an Eulerian model, it was then assumed that the actual population growth rate in the euphotic layer is given by the maximal growth rate J (Eq. 21, controlled by the mean irradiance in this layer), corrected by the fraction L_M of the cells which actually growth and divide at this rate (Eq. 3). In the present study, we assume that L_M remains constant when $Z_M > 2Z_E$ and equal to a typical value of 10%. Moreover, in order to cover the transition period between the pure winter regime ($Z_M > 2Z_E$) and the bloom regime ($Z_M < Z_E$), we assume that L_M varies linearly with Z_M/Z_E, from 10% to 100%. A sensitivity study to this parameterization is presented in Section 5.

iii. Zooplankton, (Eq. 4–5). The need to explicitly represent the detritus export as seen by sediment traps (large particles) has motivated the choice of two zooplankton compartments. We name these microzooplankton and mesozooplankton, with the following functional definitions: microzooplankton feed on phytoplankton, bacteria and detritus; mesozooplankton feed on phytoplankton, microzooplankton and detritus, and contribute to the sinking export. The formulation of the grazing terms (Eq. 22), weighted food preferences (Eq. 23) and total food availability (Eq. 24) are conceptually similar for the two zooplankton compartments. This formulation is basically that of FDM, and relies on the assumption that zooplankton feed preferentially on the most abundant food organisms. The zooplankton growth also depends on temperature, following the Simonot (1988) function (Eq. 25). The assimilated fraction of total grazing supports the growth, while the nonassimilated fraction is excreted as fecal pellets. Microzooplankton fecal pellets are entirely directed toward the small particle compartment, whereas mesozooplankton fecal pellets are considered large particles. Zooplankton liquid excretion is partitioned into ammonium and DOM. As microzooplankton graze partly on bacteria (characterized by a low C:N ratio), there is a surplus in nitrogen uptake compared to carbon: as in Drange (1994), that surplus is directed toward the ammonium pool (last term of Eq. 2). Zooplankton mortality represents natural mortality as well as predation by implicit higher predators. Zooplankton carcasses supply the small particle compartment. To avoid zooplankton total extinction during winter, under a zooplankton concentration threshold (Z_s^{min} and Z_l^{min} for micro and mesozooplankton, respectively), excretion and mortality are set to zero.

iv. Bacteria, (Eq. 6). Bacteria in the model remineralize DOM into ammonium. Labile DOM is uptaken following Eq. 26–28, while an ammonium uptake is also considered (Eq. 26–27), to insure nitrogen balance. Formulations of equations 26 to 28 comes from FDM, corrected by Drange (1994) based on considerations concerning C:N ratios of bacteria. Bacteria fuel the ammonium compartment by mortality, and are grazed by microzooplankton.

v. Particulate organic matter, (Eq. 7–8). Detritus consists of fecal material and dead organisms. Their sizes and sinking velocities vary from several orders of magnitude (cf. Andersen and Nival, 1988b, for a review). Previous studies (FDM, Fasham *et al.,* 1993; Prunet *et al.,* 1996; Sarmiento *et al.,* 1993) have shown that if only one size of detritus is considered, its sinking velocity could entirely determine the ecosystem equilibrium. Moreover, Small *et al.* (1987) have observed that tiny microzooplankton pellets do not sink but are remineralized or reingested *in situ,* whereas pellet flux is achieved by mesozooplankton. Thus, in the present model, the two detritus compartments differ by their specific breakdown rates and sinking velocities. Only small detritus is grazed, as large particles rapidly sink out of the productive layer. Small particle aggregation and large particle disaggregation are not considered here.

vi. Dissolved organic matter, (Eq. 9–10). The oceanic DOM pool is still poorly known. The most labile molecules enter the so called "microbial loop" since they are easily broken down by bacteria (Ducklow and Carlson, 1992; Fuhrman, 1992), while more refractory compounds last long enough to be exported to the deep ocean where they are slowly remineralized (over months to centuries, Ducklow *et al.,* 1995). In spite of this diversity, only two DOM compartments will be considered in the present study: labile DOM, supporting the microbial loop and refractory DOM, exportable from the surface layer. In the model, total DOM produced by phytoplankton exudation, release by zooplankton and detritus breakdown is mainly directed to the labile pool, and to a lesser extent to the refractory pool. Refractory DOM removal from surface waters is carried out by vertical diffusion and winter mixing. Some degradation of refractory DOM to labile DOM is allowed.

c. Choice of the BIOMELL parameters for DyFAMed

The ecosystem equations contain about fifty parameters which are listed in Table 2 with the standard run values. The physical and bio-optical parameters can be found in Gaspar *et al.* (1990) and Morel (1988; 1991). The assignment of values for biological parameters is a difficult task. The most satisfactory way of approaching this issue is through data assimilation (Prunet *et al.,* 1996), when the data coverage is good enough. Taking into account the large number of parameters at play, and important gaps in the dataset (for zooplankton or bacteria for instance), we have followed a more classical approach. We use parameters for which either generic values (from FDM; Prunet *et al.,* 1996), or specific values for the Mediterranean Sea (from Andersen and Nival, 1988a,b) are available. The remaining parameters were tuned to predict the seasonal cycle of nitrogen for the DyFAMed station, for which a significant amount of physical and biological data have been acquired since 1987. In the following, particular attention is paid to the parameters which have been modified from the set given by Prunet *et al.* (1996) and FDM.

i. Nutrient parameters. Previous modeling studies have employed half-saturation constants for nutrients often larger than 0.1 mmole N m^{-3} (FDM; Doney *et al.,* 1996; Prunet *et al.,* 1996). Larger values for nitrate than for ammonium were used, despite the inhibition effect of ammonium on nitrate uptake. However, recent observations emphasize the overestimation of these parameters, and strong nutrient limitation, even at the low concentrations of oligotrophic regimes, is questionable (Harrison *et al.,* 1996). Moreover, assimilation of the Bermuda Atlantic Time Series (BATS) data has led Hurtt and Armstrong (1996), from which the nutrient uptake formulation comes from, to vary the half saturation constant for ammonium (K_{nh4}) from 0.01 mmoleN m^{-3} to 0.002 mmole N m^{-3}, when additional constraints on ammonium concentrations are used. Therefore, the value chosen here (0.007 mmoleN m^{-3}) takes into account these considerations. Results are not sensitive to K_{nh4} variations between 0.004 and 0.01 mmole N m^{-3}.

ii. Phytoplankton parameters. At DyFAMed, sediment trap data (Miquel *et al.,* 1994) indicate that the C:N mole ratio is relatively constant. It increases with depth from a mean of 7.3 at 80 m to 7.6 at 200 m and 8.4 at 2000 m, presumably because of the faster degradation of nitrogen compounds relative to carbon. In BIOMELL, the classical mean value of 6.56 (105:16) is adopted and is used to convert model outputs from nitrogen units to carbon units (Takahashi *et al.,* 1985). Note that this ratio does not appear in the equations, even though the growth rate derived from Morel (1991) is in mgC $(mgChl)^{-1}s^{-1}$, while the model currency is nitrogen. This difference in units implies that the phytoplankton growth rate must be divided by the C:N ratio, while phytoplankton biomass must be multiplied by the same ratio before being converted to chlorophyll units by variable C:Chl ratio. The threshold value PUR_{max} has been chosen empirically close to the $KPUR_{opt}$ value used in the bio-optical model. The C:Chl ratio is bounded between 30 and 150 mgC $(mgChl)^{-1}$, which are in the range of extreme measured values (between 20 and 200 mgC $(mgChl)^{-1}$, Cloern *et al.,* 1995).

iii. Zooplankton parameters. Earlier studies have shown that model simulations are above all sensitive to grazing variations (Fasham, 1995; Frost, 1987). Here the microzooplankton grazing rate has been tuned to obtain a satisfactory seasonal cycle of phytoplankton (cf. section 5). The value of 1 d^{-1} is held, which is the value used in FDM, and the upper value constrained to be compatible with the occurrence of a spring bloom in subarctic oceans (Fasham, 1995). Zooplankton is assumed to feed preferentially on live matter. Therefore, their preference for detritus is set to 20%. Moreover, microzooplankton is assume to graze preferentially on phytoplankton rather than on bacteria. Nival *et al.* (1975) reported winter values of larval abundance measured with 50 μm mesh size, and found, in units of nitrogen, a value of about 0.03 mmoleN m^{-3}. On this basis, considering that the mesh size samples mainly mesozooplankton, the winter threshold values for microzooplankton (Z_s^{min}) and mesozooplankton (Z_l^{min}) are set respectively to 0.0075 and 0.0225 mmole N m^{-3}.

Table 2. Parameters of the BIOMELL model, together with the values assigned for them in the standard simulation. Parameters for which sensitivity studies are discussed in the paper are identified with an *.

Nutrients parameters			
half-saturation constant for ammonium*	K_{nh_4}	0.007	mmole m^{-3}
nitrification rate*	R_{nh_4}	0.05	d^{-1}
Phytoplankton parameters			
maximal photosynthesis efficiency	$\psi_{\mu max}$	0.07	moleC (mole quanta)$^{-1}$
gross absorption	a^*_{max}	32	m^2 (gChl)$^{-1}$
minimum Carbon/Chlorophyll ratio*	$R^{min}_{c\text{-}chl}$	30	mgC (mgChl)$^{-1}$
maximum Carbon/Chlorophyll ratio*	$R^{max}_{c\text{-}chl}$	150	mgC (mgChl)$^{-1}$
maximum PUR for C:Chl adaptation*	PUR_{max}	90	μE m^{-2} d^{-1}
optimal PUR	$KPUR_{opt}$	35	μE m^{-2} d^{-1}
Photoinhibition parameter	β	0.01	
optimal photosynthesis temperature	T^{opt}	15	°C
Van't Hoff coefficient	a_T	1.065	
phytoplankton exsudation fraction	γ	0.05	
phytoplankton mortality rate	m_p	0.078	d^{-1}
phytoplankton C:N ratio	$R^{phy}_{c:n}$	6.57	moleC (mole N)$^{-1}$
Zooplankton parameters			
optimal temperature for zooplankton growth	T^{opt}	15	°C
maximal temperature for zooplankton growth	T_{max}	35	°C
width of zooplankton temperature function	R_g	20	°C
microzooplankton maximum grazing rate*	g_{z_s}	1.0	d^{-1}
half saturation constant for microzooplankton grazing	K_{z_s}	1	mmole N m^{-3}
mesozooplankton maximum grazing rate*	g_{z_l}	0.22	d^{-1}
half saturation constant for mesozooplankton grazing	K_{z_l}	1	mmole N m^{-3}
microzooplankton preference for phytoplankton	$\breve{p}^p_{s_s}$	0.5	
microzooplankton preference for bacteria	$\breve{p}^b_{z_s}$	0.3	
microzooplankton preference for detritus	$\breve{p}^{d_s}_{z_s}$	0.2	
mesozooplankton preference for phytoplankton	$\breve{p}^p_{z_l}$	0.4	
mesozooplankton preference for microzooplankton	$\breve{p}^{z_s}_{z_l}$	0.4	
mesozooplankton preference for detritus	$\breve{p}^{d_s}_{z_l}$	0.2	
assimilated phytoplankton by microzooplankton	$a^p_{z_s}$	0.7	
assimilated bacteria by microzooplankton	$a^b_{z_s}$	0.7	
assimilated detritus by microzooplankton	$a^{d_s}_{z_s}$	0.5	
assimilated phytoplankton by mesozooplankton	$a^p_{z_l}$	0.5	
assimilated microzooplankton by mesozooplankton	$a^{z_s}_{z_l}$	0.5	

Table 2. (Continued)

assimilated detritus by mesozooplankton	$a_{z_l}^{d_s}$	0.3	
ammonium fraction of microzooplankton excretion	ϵ_{z_s}	0.75	
ammonium fraction of mesozooplankton excretion	ϵ_{z_l}	0.75	
microzooplankton excretion rate	μ_{z_s}	0.1	d^{-1}
mesozooplankton excretion rate	μ_{z_l}	0.02	d^{-1}
microzooplankton mortality rate	m_{z_s}	0.037	d^{-1}
mesozooplankton mortality rate	m_{z_l}	0.018	d^{-1}
microzooplankton concentration threshold*	$Z_s^{\min}$	0.0075	mmole N m^{-3}
mesozooplankton concentration threshold*	$Z_l^{\min}$	0.0225	mmole N m^{-3}
Bacteria parameters			
maximum bacterial uptake rate	V_b	2.0	d^{-1}
bacteria half-saturation uptake constant	K_b	0.5	mmole N m^{-3}
ratio of DOM to ammonium bacterial uptake	η	0.6	
bacterial mortality rate	m_b	0.05	d^{-1}
bacterial C:N ratio	$R_{c:n}^{bac}$	4.2	mole C (mole N)$^{-1}$
DOM parameter			
labile DOM fraction*	f_{dom_l}	0.75	
refractory DOM breakdown rate	μ_{dom_r}	1	y^{-1}
refractory DOM C:N ratio	$R_{c:n}^{dom}$	12	mole C (mole N)$^{-1}$
Detritus parameters			
sedimentation speed for small detritus	V_{d_s}	1	m d^{-1}
sedimentation speed for large detritus	V_{d_l}	100	m d^{-1}
small detritus breakdown rate	μ_{d_s}	0.1	d^{-1}
large detritus breakdown rate	μ_{d_l}	0.033	d^{-1}

iv. Detritus parameters. At the DyFAMed site, Miquel *et al.* (1994) derived a mean particle settling velocity of at least 92 m d^{-1} from mass flux data at three different depths. As the sediment traps catch only large particles, a value of 100 m d^{-1} is chosen for the large particle sinking rate. The settling velocity of small particles is set to 1 m d^{-1}, a medium value taking into account the settling velocity of diatom cells (0.1 to 2.1 m d^{-1}, Andersen and Nival, 1988b) and of smaller particles, which are known to contribute to approximately 95% of the total particle mass and have settling velocities lower than 1 m d^{-1}. Breakdown rates are $(10\ d)^{-1}$ for small particles and $(30\ d)^{-1}$ for larger ones. These values, considering the respective sinking velocities, allow small particles to be almost entirely remineralized within a 100 m depth layer, and large particles to contribute mainly to the export.

v. DOM parameter. The f_{dom_l} ratio is the percentage of total DOM directed toward the refractory DOM compartment, the remainder feeding the labile DOM compartment. Its value (15%) has been determined by trial-and-error simulations to reproduce the observed DOC export (see Section 5). The decay time constant towards labile DOM is set to one year, which allows accumulation during the oligotrophic summer. A C:N ratio of 12 is used to validate the export against data.

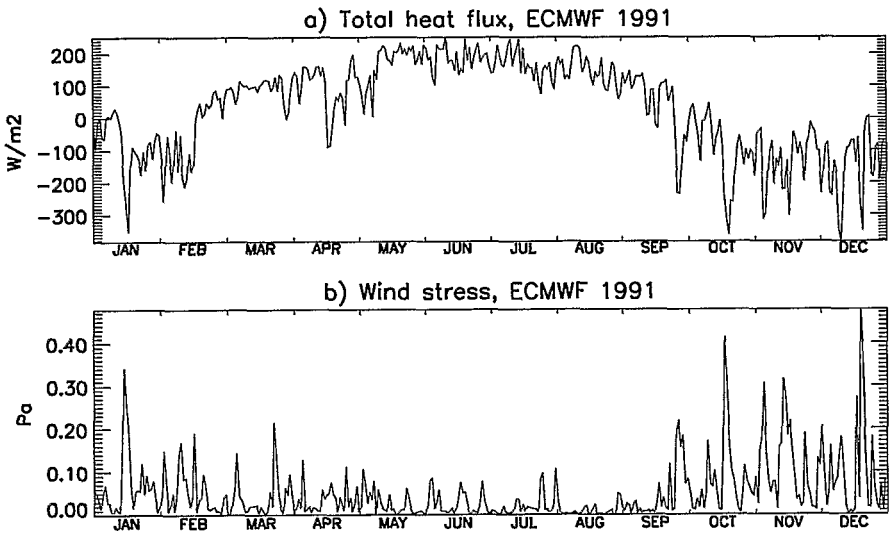

Figure 3. Daily averages of (a) net heat flux in Wm^{-2} (with an albedo of 0.03) and (b) strength of the wind stress in Pa, from 1991 ECMWF simulations over the DyFAMed station.

d. The 1991 simulation at DyFAMed.

The first three hundred meters of the water column are covered with a five meter vertical resolution. Initialization is done with DyFAMed data from January 24, 1991, except when not available, i.e. for zooplankton, bacteria, detritus, ammonium and labile DOM, which are set to small positive concentrations in order to enable their growth (10^{-6} mmole N m^{-3}). The model is run on a perpetual 1991 year, until steady state is achieved for all variables. Steady state is obtained during the first two years, and all the presented model results are from the third year of simulation.

Surface layer dynamics are derived from the turbulent kinetic energy model (TKE) of Gaspar *et al.* (1990) at all depths. It is driven by the forcing fluxes provided by the European Center for Medium-Range Weather Forecast (ECMWF) for 1991 (Fig. 1 and 3). Six hourly estimates are available, making this forcing suitable to high frequency studies. Winds and heat fluxes resulting from Atmospheric General Circulation Models can be strongly in error: as an example, it is well known that ECMWF overestimates the short wave radiation, due to poor representation of clouds. Therefore, the formulation of the surface fluxes is similar to the one generally used in Ocean General Circulation Models: a damping term driving the sea surface temperature towards the data is added to the ECMWF estimates of the fluxes. Nevertheless, the annual heat budget is not closed. Even at a location like DyFAMed, supposed to be mostly 1D, horizontal advection can explain part of that drift. Very few data are available to estimate the period of the year when 3D dynamics could modify the vertical structure at DyFAMed, which makes corrections difficult to introduce. However, winter convection and restratification during spring are

mostly 3D processes (Gascard, 1978). Moreover, winter can be considered as the initial condition for the annual cycle. Finally, during convection, profiles are rather homogeneous. Therefore, during 30 days, before day 40, for which data are available and which is not far from the time when the mixed layer is the deepest in the model, the temperature profile is forced toward observations using a simple nudging technique. Also, because there is no surface salinity forcing available, the same technique is applied to salinity. We are aware of the questions that can be raised by that very crude parameterization, but that solution seems to be a reasonable compromise for this 1D study, taking into account the lack of data, and the intrinsic 3D behavior of the ocean. This solution prevents system drift. The vertical diffusion coefficients k_z derived by the TKE model are used to estimate the vertical diffusion fluxes of biogeochemical tracers. The mixed-layer is defined as the surface layer where k_z remains higher than 10^{-5} m^2 s^{-1}.

Because the model is closed at the bottom (300 m), the model cannot by itself achieve steady state as it loses nitrogen by particulate sedimentation and refractory DOM accumulation. In order to obtain steady state, nitrate and refractory DOM are relaxed towards their profiles at day 40, with a one-month time scale, thus providing nitrate and exporting DOM from the system. As for temperature, this nudging can be interpreted as a mean of replacing 3D effects during this period and thus accounts for winter mixing. Comparisons with a simulation with no nudging have shown that nudging induces no modification of the system behavior, and actually only prevents its drift. This result is not surprising, since nitrate is not limiting in December, and refractory DOM has a weak feedback on the biogeochemical system.

4. Comparison of the model output with data

The first step of the validation is made using data obtained in 1991 approximately every month. Temperature, chlorophyll and nitrate profiles were acquired at the DyFAMed station, from CTD, fluorescence and nutrient analyses, respectively (DyFAMed, 1995). Extended datasets from different years is also used to validate seasonal variations of other variables, for which the coverage in 1991 was poor: zooplankton, sediment traps and DOC.

a. Hydrography

Simulated seasonal temperature evolution is compared to interpolated 1991 *in situ* profiles (Fig. 4). Seasonal variations are well reproduced: in winter, the temperature is uniform in the water column and below 13°C. In spring, isotherms rapidly deepen (in the model, this happens at the precise time when the forcing heat flux becomes positive). Between spring and summer, the progressive warming of the surface induces maximum stratification of the water column. Destratification in fall is more progressive than stratification in spring (which is obvious in the model mixed-layer depth, Fig. 5). Nevertheless, even though the slope of the isotherms are comparable, the summer thermocline is more diffused in the model than in the data. This suggests that the TKE

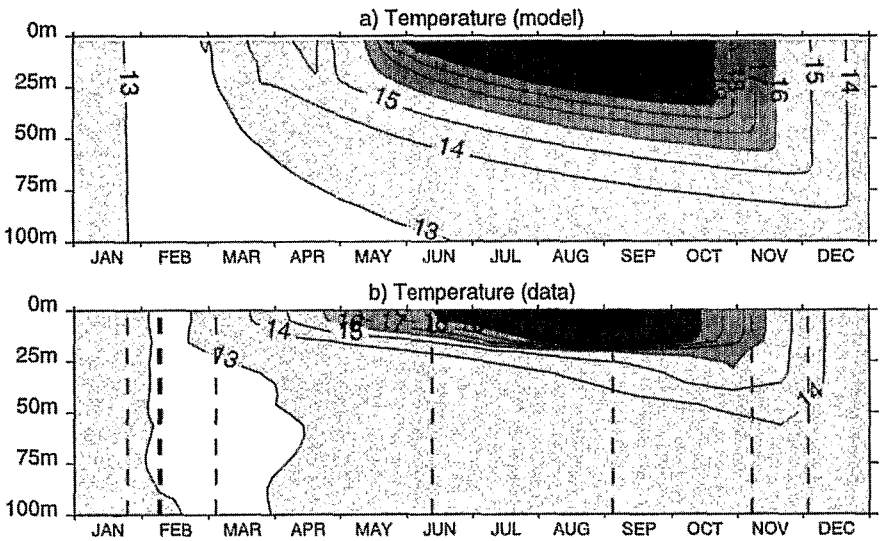

Figure 4. (a) Simulated temperature for 1991. (b) Temperature data measured at the DyFAMed station in 1991, interpolated in time and depth. Dotted lines show the eight measured profiles.

derived diffusion coefficients might be overestimated in the summer thermocline. Comparisons of the heat budgets between the data and the model show that the increase (decrease) during summer (fall) is too large in the model by several Wm^{-2}, which means that, in summer, either the ECMWF fluxes are too large, or that 3D processes cool the water column. The simulated mixed layer is also in good general agreement with the mixed layer

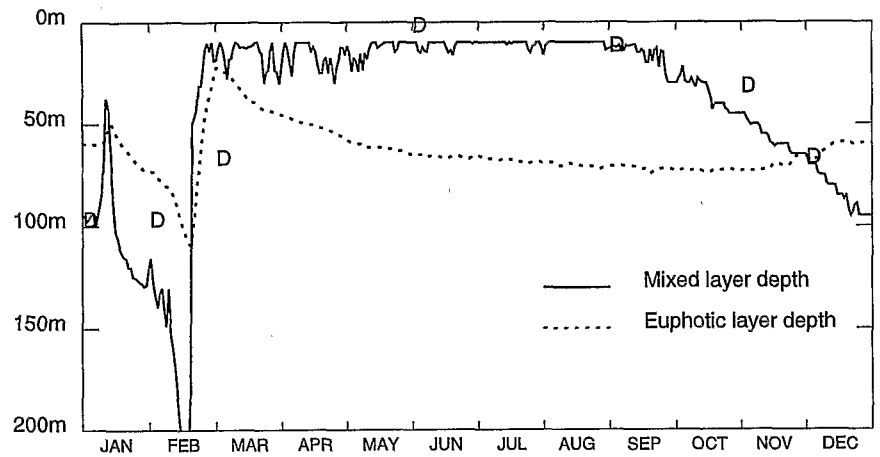

Figure 5. Simulated mixed layer depth (solid line, using the criteria that $k_z > 10^{-5}$ m^2 s^{-1}) and euphotic layer depth (dotted line, 1% of incident illumination). Mixed-layer depth estimates from CTD data (using the criteria that the density gradient between the surface and the base of the mixed layer is 0.05) are shown by the capital letter D.

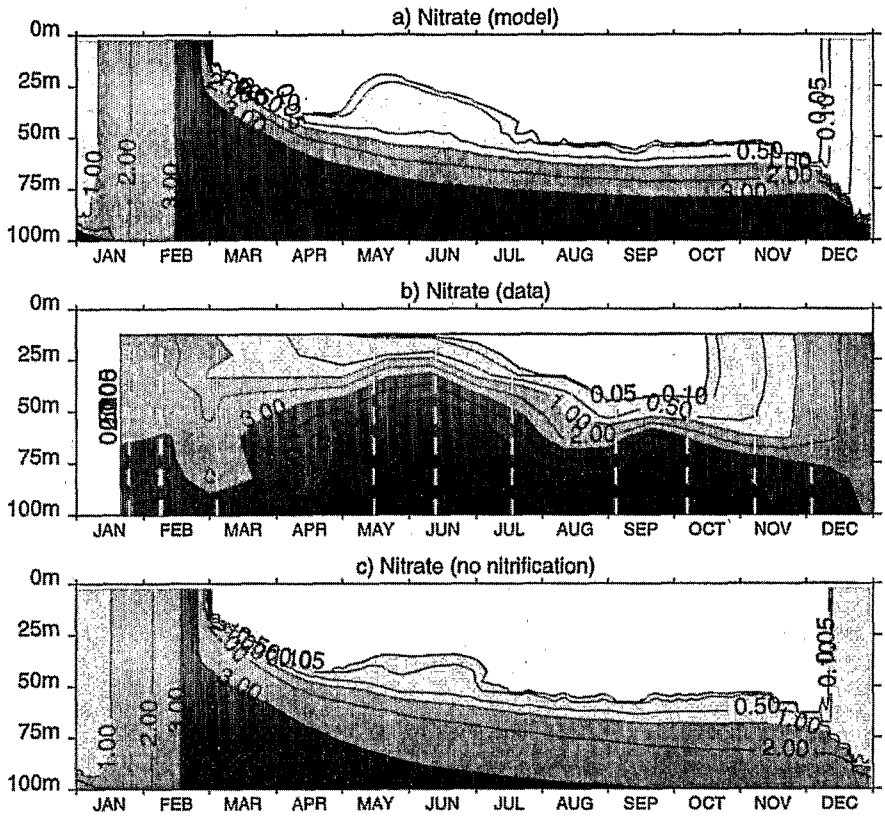

Figure 6. (a) Simulated nitrate for 1991. (b) Nitrate data measured at the DyFAMed station in 1991 (with a detection limit of 0.05 mmole N m^{-3}) interpolated in time and depth. Dotted lines show the ten measured profiles. (c) Simulated nitrate in a sensitivity experiment where nitrification is not accounted for. Units are mmole N m^{-3}.

estimated from *in situ* density profiles (Fig. 5). One exception is the early March estimate; the model restratifies too early, which again could either be due to shortcomings in the forcing or to 3D processes. However, we will assume that the physics derived from the 1D model is satisfactory for the purposes of this study.

b. Standing stocks: mean seasonal variability

The time evolution of the simulated nitrate, phytoplankton and chlorophyll are shown Figures 6a, 7a and 7b. Phytoplankton evolution is mainly controlled by nutrient and light (mixed-layer depth) availability, and grazing. From mid-January to the end of February, nutrients that have been brought up to the surface by winter mixing are fully available (Fig. 6a). The mixed-layer is much deeper than the euphotic layer (Fig. 5), and the strong and permanent mixing inhibits photosynthesis: it is a typical winter regime, as observed by Gostan and Nival (1963). This strong, deep mixing induces low C:Chl ratio, close to its

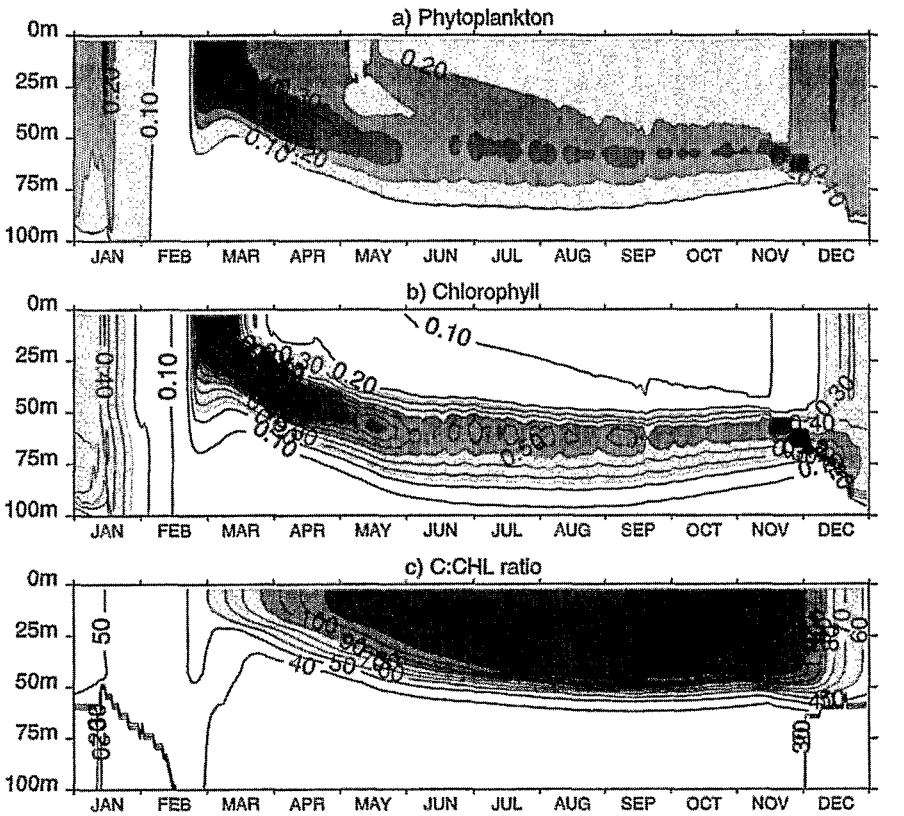

Figure 7. Annual cycle of simulated (a) phytoplankton (in mmole N m^{-3}), (b) chlorophyll (in mgChl m^{-3}) and (c) C:Chl ratio (in mgC$(mgChl)^{-1}$) for 1991.

lower bound (Fig. 7c). As soon as the water column is stratified (Fig. 5), phytoplankton start to grow and a bloom occurs, followed by a strong microzooplankton production (Fig. 8a) about a month later, and mesozooplankton production one month after that (Fig. 8b). This succession of species is consistent with observations (Jacques, 1988), and analysis of specific composition of fatty acids in sediment traps (Marty *et al.*, 1994b). From these analyses, a high biological production was found in spring and early summer, with highest phytoplankton debris in March–April, but highest zooplankton debris in late June and July. In summer and early autumn, the simulated system is characteristic of oligotrophy, with a surface-depleted nutrients (Fig. 6a), a DCM (Fig. 7b) located in the nitracline, and high C:Chl ratio in the upper ocean (Fig. 7c). This oligotrophic regime has first been discussed by Jacques *et al.* (1976), and is also obvious in the DyFAMed (1995) dataset. Destratification causes new nutrient supply and a late autumn secondary bloom (Fig. 5, 6a, 7a), clearly seen in the 1991 observations. In mid-January, a short bloom is observed (Fig. 7a) due to a short event of restratification of the upper ocean (Fig. 5). This event is likely related to winter diatom blooms (Marty, 1993). Pigment biomarker analyses

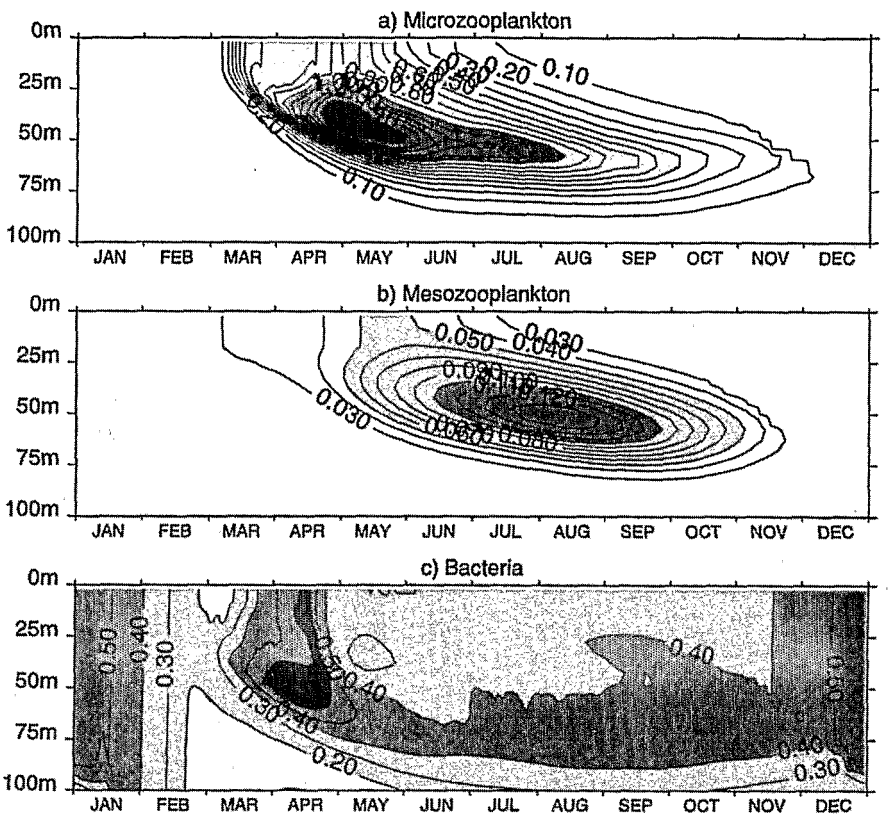

Figure 8. Annual cycle of simulated (a) microzooplankton, (b) mesozooplankton and (c) bacteria for 1991. Units are mmole N m^{-3}.

(Claustre, 1994; Marty, 1993) have also distinguished among seasonal regimes. Divinyl-chlorophyll identified from August to November is characteristic of prochlorophytes, strongly associated to oligotrophy; fucoxanthine, abundant from December to March, is characteristic of diatoms, indicating strong mixing; and flagellate pigments, observed during April–June, are evidence for stratification.

c. Standing stocks: comparison with data

Figure 6 shows the comparison between simulated nitrate with full model resolution and data in 1991 linearly interpolated to model resolution in both directions (time and depth). The general patterns are reasonably reproduced by the model: in particular, the formation of a sharp nitracline in April and its deepening throughout the year. Low summer surface values are also consistent with data.

Above 50 m, the model simulates a strong nitrate depletion in April, followed by an increase in nitrate concentrations in May. The depletion is correlated to the spring

phytoplankton bloom (Fig. 7a). The increase in May is due to nitrification, the major nitrate source at this time of the year (Fig. 13), consistent with high ammonium levels just after the phytoplankton bloom (Fig. 16) and during the growth phase of microzooplankton (Fig. 8a). On March 7, nitrate surface concentrations are lower in the model than in the data, which could mean that the bloom starts a few days too early in the model. This is consistent with the fact that stratification starts earlier in the model than in the data (Fig. 5). On May 16, nitrate profiles are quite similar in the model and in the data; nevertheless, due to the time resolution of the data (no data between March 7 and May 16), the increase of nitrate concentration in May is not obviously seen in the dataset.

During fall, the increase in nitrate observed in the data occurs earlier than in the model. At the end of summer, the mixed layer begins to deepen, but it is not until the beginning of December that its depth reaches the nitracline. Therefore, the model cannot supply the upper ocean with nitrate before that time. The shift could be due either to shortcomings in the 1D dynamics, or to overestimation of the nitrate uptake during summer. Simulations performed with a modified representation of the nutrient limitation, or with different parameters associated with primary production, led us to the conclusion that the structure of the biological model itself cannot reproduce the increase in the surface nitrate concentration in October. It is more likely that the dynamics (vertical velocities, mesoscale activity) could explain the differences between the data and the model results.

Figure 9 compares chlorophyll results with time and depth interpolated data. Besides the general good behavior of the model, four points are emphasized by this figure. In winter, although the simulated chlorophyll is low, it is about twice as large as the data. These results are very sensitive to the parameters associated with the C:Chl ratio (PUR_{max}, $R_{C:Chlmax}$, $R_{C:Chlmin}$). Small increases of $R_{C:Chlmin}$ or decreases of PUR_{max} lower the chlorophyll values in winter.

Between March 7 and May 13, no data are available; maximum surface chlorophyll values of 2 to 3 mgChl m^{-3}, as detected from satellite sensors (André, 1990), have been missed. These concentrations are obtained with the model, which simulates a clear spring bloom in March. Figure 9b confirms that the bloom occurs several days too early in the simulation. As the bloom starts very suddenly and at the precise moment when the mixed-layer depth decreases sharply in spring, the time lag is not believed to be very significant.

The intensity of the DCM is well reproduced by the model, but in early summer, this maximum is too deep and in late summer too shallow. In the model, the DCM is closely associated with the position of the nitracline and the C:Chl ratio gradient. With constant parameters all along the year, the model is not able to reproduce large variations of the DCM depth. Succession of species and vertical layering of phytoplankton populations (Pollehne *et al.*, 1993), with different C:Chl values, can modify the evolution of the vertical structure of chlorophyll, and partly explain the trend in the DCM depth. However, June is characterized by an uplift, and September by a downward deflection of the deep nitrate field (Fig. 6b). Though not clear from the temperature distribution, vertical movements

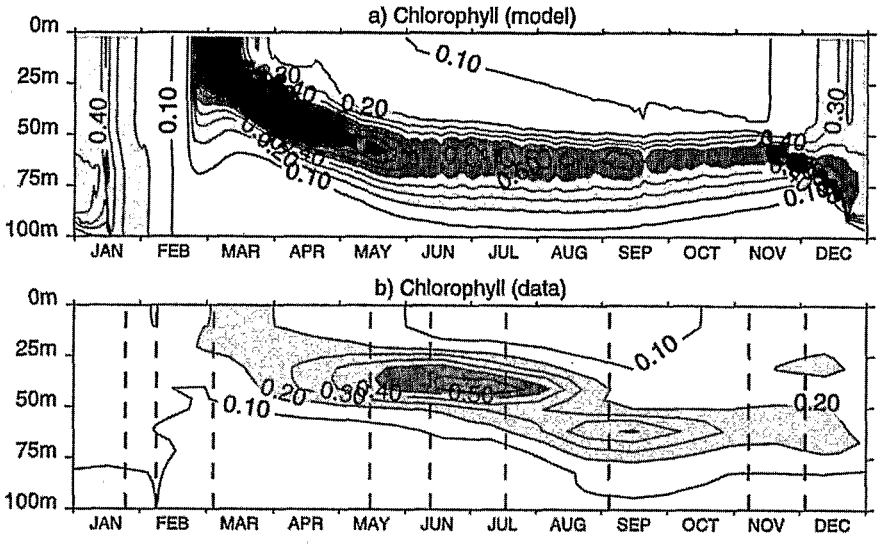

Figure 9. (a) Simulated chlorophyll for 1991. (b) Chlorophyll data measured at the DyFAMed station in 1991, interpolated in both time and depth. Dotted lines show the nine measured profiles. Units are in mgChl m^{-3}.

could be responsible for such patterns. Numerical experiments have shown that average vertical velocities of less than 1 md^{-1} during a week or two are able to create displacements of about 10 m in the nitrate and chlorophyll fields (Lévy, 1996).

During the second half of November, the model exhibits an increase of chlorophyll at 60 m. That short event occurs just when the mixed layer reaches the depth of the nitracline, which is close to the euphotic zone depth at this time of the year (Fig. 5). Light and nutrients are sufficient to locally stimulate production. As the mixed layer deepens more and more, the chlorophyll patch is quickly diluted afterwards.

It is almost impossible to compare the simulated zooplankton cycles to observations as we know of no comprehensive sampling of zooplankton at DyFAMed. Nival *et al.* (1975) sampled zooplankton along the Nice-Calvi transect during two of the 15-day legs of the Mediprod-I Program, the first, in March, the second, in April. They used vertical net hauls (mesh size 200 μm) over a depth range of 0–75 m. They reported very low zooplankton concentrations during the first, late winter cruise, with dry weights of about 5 mg m^{-3}, and much higher concentrations (about 60 mg m^{-3}) from the surface down to 50 m during the second, spring cruise. Converting these data to nitrogen units (according to Nival *et al.*, 1975) gives a variation from 0.024 mmole N m^{-3} in winter to 0.28 mmole N m^{-3} in spring. Scarce additional zooplankton measurements in other parts of the North Mediterranean Sea show similar zooplankton variations. Alcaraz (1988) reported mean summer values of 0.06 mmoleN m^{-3} in the Balearic Islands, while Razouls and Kouwenberg (1993) encountered a May–June zooplankton maximum of 0.2 mmole N m^{-3} and a winter minimum of 0.05 mmole N m^{-3} in the Gulf of Lion. The simulated mesozooplankton

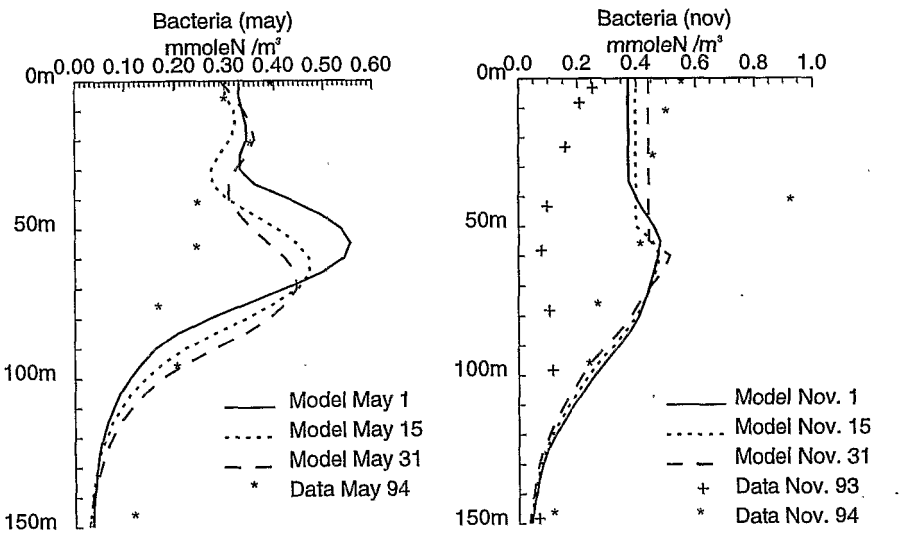

Figure 10. Simulated and measured bacteria profiles at DyFAMed, in May and in November. Units are mmole N m^{-3}.

concentrations show a maximum of 0.14 mmole N m^{-3} occurring in June, within the range of the reported data, and with a good timing. Clearly, data on microzooplankton stocks are important for further calibration of this model.

Several authors (Cho and Azam, 1990; Krstulovic *et al.,* 1995) have shown that with increasing oligotrophy, phytoplankton biomass is far below bacterial biomass, while in eutrophic waters, bacterial biomass is generally much smaller than phytoplankton biomass. Compared bacteria and phytoplankton concentrations (Fig. 7a and 8c) show that the model agrees with this general pattern during the bloom, as well as in summer. Integrated over the first 100 m in nitrogen units, the ratio of the bacterial and phytoplanktonic biomasses is equal to 0.66 during the bloom and 2.20 during the summer (0.42 and 1.40 in carbon units). We only dispose of three bacteria profiles from the DyFAMed station (Fig. 10, L. Guliano, pers. comm.). The two measured profiles in November are very different. Besides the pick at 50 m, the 1994 one is similar in distribution and order of magnitude to the simulated bacteria for November 1991, while the 1993 one is smaller by a factor two. The profile from May 1994 has again the right order of magnitude, although the model results show a maximum at 75 m not seen in the data.

Vertical profiles of DOC content were obtained monthly at the DyFAMed site (starting from July 1991), using a high temperature catalytic oxidation method (Avril, 1995). A composite year made out of these profiles (Fig. 11b) show an excess of DOC in surface waters increasing from February to October. The simulated refractory DOC profiles (Fig. 11a) also show this accumulation though the year. The range of variation simulated in the surface layers agrees with the data. Nevertheless, the vertical gradient is too small, and the maximal surface accumulation of DOC is reached about a month later in the simulation.

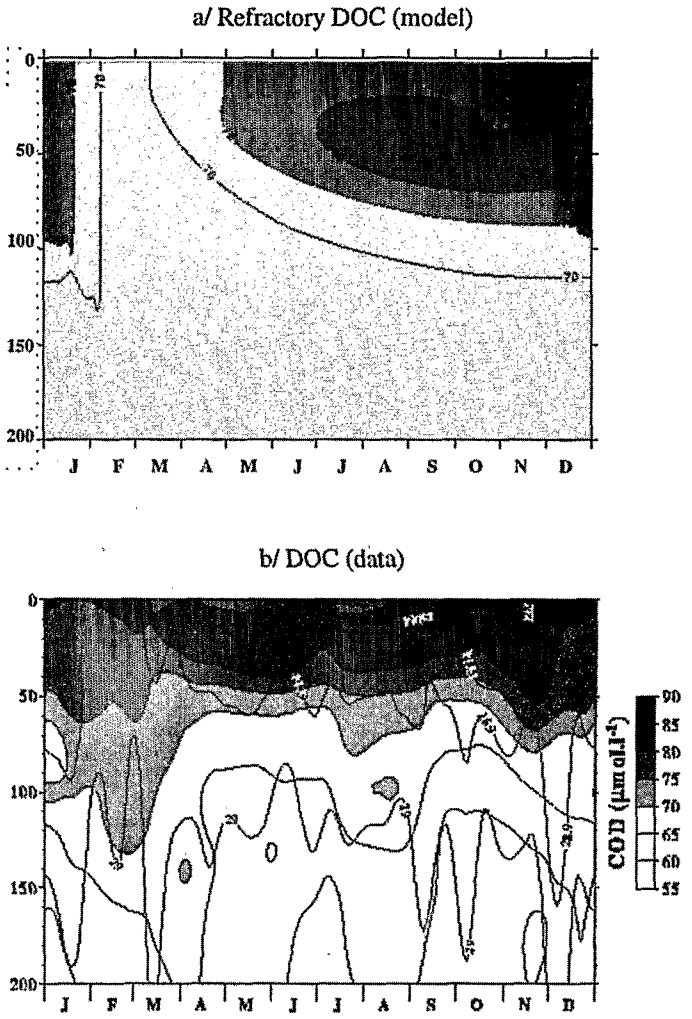

Figure 11. (a) Simulated refractory DOM annual cycle for 1991, converted to carbon units using a C:N constant ratio of 12. (b) Composite year of DOC concentrations derived from measurements at DyFAMed from 1991 to 1994 (from Avril, 1995). Units are mmole C m^{-3}.

By construction (damping toward a homogeneous profile in winter) and due to strong mixing in the deep mixed layer in winter, there is no DOC vertical gradient in February–March in the model (as for nitrate). The time shift in the decrease of the accumulation of surface DOC may be compared with the same shift in nitrate increase (Fig. 6a), which could imply shortcomings in the deepening of the mixed layer in fall. However, the crudeness in the representation of DOC in the model, and problems raised by the definition of labile and refractory DOM, must obviously be considered as well.

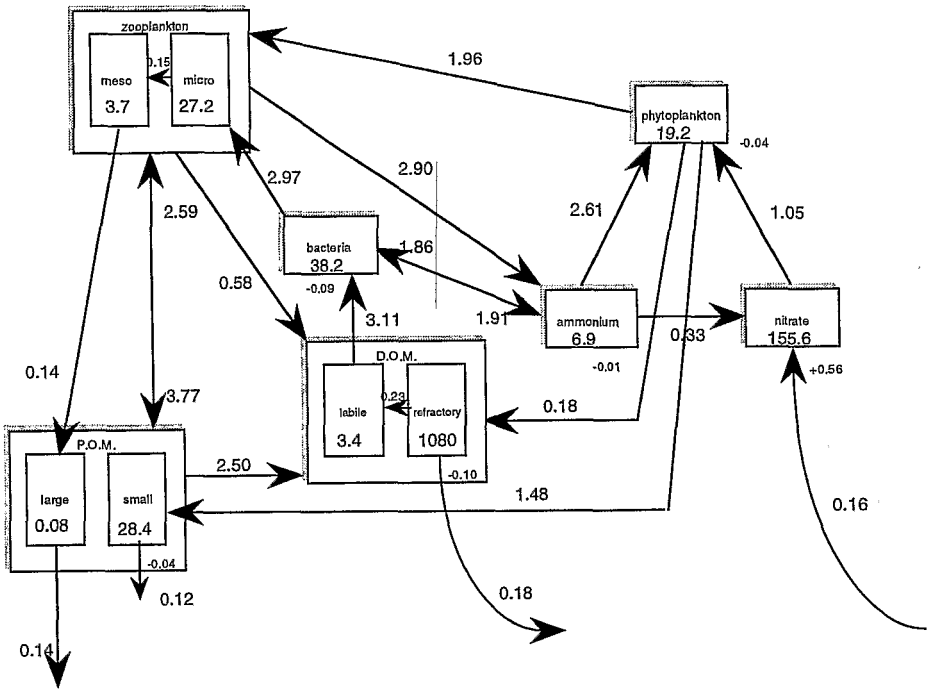

Figure 12. Mean annual concentrations (mmole N m^{-2}) and mean fluxes (mmole N m^{-2} d^{-1}) in the first 100 m. Mean concentrations are indicated within each compartment. The smaller figures underneath indicate the vertical diffusion trend of the compartment (when not negligible), while biogeochemical trends between two compartments are indicated over the arrow between these compartments, the direction of the arrow accounting for the sign of the trend (positive for a source, negative for a sink). Nudging trends are those close to bent arrows. The factor used to convert mmole N m^{-2} d^{-1} to the carbon units given in the text (gC m^{-2} y^{-1}) is 12 × 6.57 × 0.365, except for DOM export which is computed using a C:N ratio of 12 instead of 6.57.

d. Production fluxes

Using ^{14}C measurements, Minas (1970) has estimated the Northwestern Mediterranean TP rate to be about 78 gC m^{-2} y^{-1}. Morel and André (1991) have derived primary production rates from satellite (CZCS) observations, and evaluated the annual rate of carbon fixation for the whole western basin to be about 94 gC m^{-2} y^{-1}. They also have provided a review of primary production measurements in the area (Bethoux, 1981, 1989; Jacques, 1988; Minas *et al.,* 1988) in good agreement with their estimate. However, using different parameter values and cloud forcing, the first estimate of Morel and André has been revised to 157.7 gC m^{-2} y^{-1} by Antoine *et al.* (1995). The simulated annual mean TP (Fig. 12, 105.5 gC m^{-2} y^{-1}) falls between these two estimates.

^{14}C measurements during Mediprod 1 yields to TP values of 387 mgC m^{-2} d^{-1} in March and 982 mgC m^{-2} d^{-1} in April. Recent TP DyFAMed data acquired once in March and once in April 1994 give higher daily estimates (~800 and 1900 mgC m^{-2} d^{-1} respectively;

J. Chiaverini, pers. comm.). Indeed, the first Mediprod 1 estimates are likely not trace metal clean and may be biased low. The model averaged predictions are much lower: 402 mgC m^{-2} d^{-1} in March, 413 mgC m^{-2} d^{-1} in April, and 501 mgC m^{-2} d^{-1} in May. An explanation could be that the time of incubation (12 h during Mediprod 1, 4 h at DyFAMed) is too short to derive the exact net production, putting the measured estimates somewhere between gross and net production, whereas the model predicts net production. An other reason could be the underestimation of total production by the bio-optical model of Morel (1991) under spring bloom conditions, as suggested by comparisons of the recent PP measurements at DyFAMed with estimates derived from the Morel (1991) model forced with *in-situ* chlorophyll (J. Chiaverini, pers comm.). It is thus difficult to say whether the model predicted spring TP is too low, or if the measurements are overestimates.

Due to nitrification, exact NP is hardly assessable from nitrate uptake. On an annual average, NP equals nitrate-based production minus nitrification, but instantaneously, nitrification can prevail over nitrate-based production, when the latter is strongly inhibited (particularly during winter). Biological activity is then is a net source of nitrate in the euphotic layer. By subtracting nitrified nitrate to total nitrate consumption by phytoplankton, both averaged over the 100 m surface layer, we obtain an annual estimate of new production of 20.9 gC m^{-2} y^{-1} (Fig. 12). The same result is obtained by summing the vertical fluxes of nitrogen over the 100 m surface layer, and then adding the winter nudging term. This value is consistent with previous estimates of NP in the Northwestern Mediterranean basin: estimating phosphate supply from deeper layers and its subsequent consumption in the euphotic layer, Minas *et al.* (1988) reported a value of 18 gC m^{-2} y^{-1}. Applying the oxygen utilization method and taking into account the annual deep water formation, Bethoux (1989) derived a value of 12–35 gC m^{-2} y^{-1}. The metabolic CO_2 production over the year 1990 yields an estimate of 18.4 gC m^{-2} y^{-1} ($\pm$40%) (Lefèvre *et al.*, 1996).

Phosphate consumption between the two one-month interval Nice-Calvi transects of Mediprod 1 gave an estimate of 247 mgC m^{-2} d^{-1} for new production during the bloom (Minas *et al.*, 1988). The mean simulated nitrate-based production during the bloom is 276 mgC $m^{-2}d^{-1}$, and is presumably very close to NP as nitrification is weak in the euphotic layer during that period (Fig. 13). The difference between the model and the data is low and could be due to interannual nitrate input variability. From the 1964 "Bouée Laboratoire" experiment, Minas and Codispoti (1993) estimated a NP of about 55 mgC m^{-2} d^{-1} in September, and 90 mgC m^{-2} d^{-1} during the summer season. The mean simulated nitrate-based productions for the oligotrophic and autumn periods are respectively 50 and 57 mgC m^{-2} d^{-1}. Although nitrification is no longer negligible, the model reproduces right orders of magnitude.

Nitrification measurements in the Almeria-Oran frontal system (Bianchi *et al.*, 1993) have shown that the nitrate resulting from nitrification is able to contribute as much as 40% of the nitrate supply for phytoplankton. They report ammonium oxidation rates varying from 10^{-3} to 4.5 10^{-2} mmole N m^{-3} d^{-1}, and a maximum of nitrite oxidation rates located

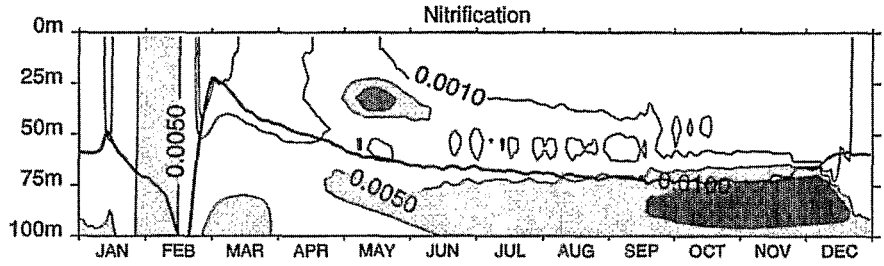

Figure 13. Daily averaged nitrogen flux between ammonium and nitrate compartments due to nitrification, units are mmole N m^{-3} d^{-1}. The plain, dark line marks the limit of the euphotic zone.

at the top of the nitracline. In the standard simulation, ammonium oxidation rates vary within the same range (Fig. 13), and nitrification sustains about 30% of the overall nitrate consumption in the first 100 m as an annual mean. We are aware this value is very controversial. However, nitrification occurs mostly in summer and autumn (about 3 times the spring value) and is maximum just below the euphotic layer, where nitrification kinetics prevails over ammonium consumption by phytoplankton. Note that this value is about three times smaller if the budget is undertaken in the euphotic layer (Fig. 5): nitrification accounts for 0.07 mmole N m^{-3} d^{-1} in nitrate production, which represents 10% of nitrate consumption.

The ratio between NP and TP cannot be derived directly from the model, but it can be bounded by the ratio between nitrate-based production and TP, and the ratio between nitrate-based production minus nitrification and TP. The mean simulated *f*-ratio for spring is 0.70. It is much higher than the 0.36 spring *f*-ratio estimated from Mediprod 1 (Minas and Bonin, 1988; Minas and Codispoti, 1993; Minas *et al.,* 1988). However, the 0.70 value seems much realistic for a bloom period when nitrate are fully available. The surprisingly low value of 0.36 has been explained by the presence of zooplankton, but this point is controversial, as zooplankton develops only one month after phytoplankton. In summer, the simulated *f*-ratio ranges between 0.10 and 0.17, characteristic of an oligotrophic regime, and it reaches 0.19 to 0.37 in autumn. The 0.5 (Minas *et al.,* 1988) estimate for summer is much higher, and surprisingly higher than the reported *f*-ratio during spring.

e. Export fluxes

What we will refer as "export" is the export of organic matter below 100 m, which is somewhat different than the "real" export to the deep ocean (Bender *et al.,* 1992). Due to their high sinking velocity (100 m d^{-1}) compared to their remineralization rate ($(30\ d)^{-1}$), large particles flux at 100 m is about the same than at 200 m. It is not the case with small particles, which are almost entirely remineralized when they reach 200 m, leading to DOM storage between 100 and 200 m.

Time series measurements of downward fluxes of settling particles have been monitored since 1987 in the framework of the DyFAMed project (Miquel *et al.,* 1993; 1994).

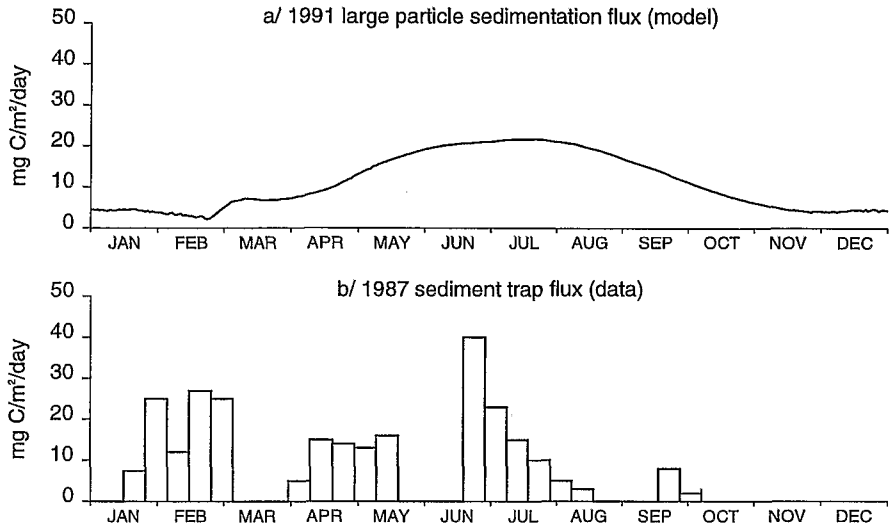

Figure 14. Large particle flux, (a) standard simulation for 1991 and (b) 200 m sediment traps data at DyFAMed for 1987, from (Miquel *et al.*, 1994). Units are mgC $m^{-2}d^{-1}$.

Automated sediment traps were used to collect samples, particularly at 200 m-depth. Figure 14 compares 1987 sediment traps measurements to the 1991 simulated large particle export calculated at 200 m, as no data are available for 1991. These two fluxes have the same order of magnitude and follow the same temporal pattern. They increase from March to May–June, and then gradually decrease. Surprisingly high winter downward fluxes, during a period where primary production is believed to be minimum, have been observed and are not simulated. They have become the focus of attention, and various explanations have been proposed. Miquel *et al.* (1994) pointed out that particle fluxes were enhanced during vertical mixing events and attributed this winter anomaly to a physical rather than biological control of the fluxes. Marty *et al.* (1994b) used organic biomarker analyses to understand the origin of these fluxes. They have found that the higher fluxes occurring during winter are associated primarily with old refractory organic matter, probably of continental origin. This second hypothesis is supported by the fact that the same temporal pattern has been observed in near shore Northwestern Mediterranean waters (Fowler *et al.*, 1991). The contribution of diatoms to the monitored vertical flux in winter could also explain the discrepancy between model results and data during that period, as phytoplankton does not directly contribute to the large detritus pool in the model.

The model annual large particle export is 3.9 gC m^{-2} y^{-1} (Fig. 12), very close to the mean monitored export (4.0 gC m^{-2} y^{-1} for the period 1987–1990). This good agreement comes partly from the fact that several critical parameters associated with mesozooplankton have been tuned (see part 5). It is interesting to note that the model predicts an export of phytoplankton through mixing processes of 0.91 gC m^{-2} in January, when a winter secondary bloom is simulated. This figure can be related to the winter vertical export of

organic matter presumably achieved through diatoms, which means that the particulate export could then be too high in the model. Similar significant export of phytoplankton by winter deep-mixing events was found by Doney *et al.* (1996). Data constraining the diatom contribution to winter export are of course needed for further conclusion. The non-parameterized processes of aggregation and disaggregation are probably responsible for an other source of error.

The model predicts an annual refractory organic matter export of 14.7 gC m^{-2} y^{-1}, mostly through winter vertical mixing (Fig. 12). Copin-Montegut and Avril (1993) have made an estimate of the DOC export on the assumption that all the DOC accumulated in the surface waters is removed by winter mixing. This led to a winter DOC export of 14.8 gC m^{-2} y^{-1}. The model reproduces DOC export quite well. This good agreement is not surprising since, for a fixed C:N ratio, the f_{dom_l} ratio value has been tuned accordingly.

The model also calculates other forms of export (Fig. 12), like small particle sedimentation (3.5 gC m^{-2} y^{-1} at 100 m and 0.15 gC m^{-2} y^{-1} at 200 m), and dead or living organism export by winter diffusion (4.2 gC m^{-2} y^{-1} at 100 m, achieved mainly by detritus, bacteria and phytoplankton, and 0.48 gC m^{-2} y^{-1} at 200 m). This last mechanism has been proposed by Nival *et al.* (1975) to close the phytoplankton consumption budget; they have found that 7% of phytoplankton and zooplankton biomasses had to be lost from the productive layer through hydrological processes.

5. Sensitivity studies

The success of a model depends first on its structure and on the parameterization of the processes involved, but also on the choice of parameter values. Here we estimate model error as a function of key or unknown parameters. In view of the large number of parameters, this study is far from being exhaustive. It only seeks to point out selected deficiencies in the present knowledge of processes that seem to be important components of the oceanic carbon and nitrogen cycles, and to point out the lack of suitable measurements to overcome these uncertainties. Percentage values given in the following discussion correspond to the sensitivity experiment estimates relative to the annual mean predictions of the standard simulation given in Figure 12.

a. C:Chl ratio

Few biogeochemical models take into account variability in C:Chl ratio (Doney *et al.*, 1996; Hurtt and Armstrong, 1996; Lawson *et al.*, 1996). However, data clearly show that this ratio can vary by one order of magnitude (Cloern *et al.*, 1995). Figure 15 shows the simulated phytoplankton and the chlorophyll distributions for a sensitivity study where the C:Chl ratio is constant and equal to 55 mgC $(mgChl)^{-1}$. During the oligotrophic summer, this sensitivity study shows that a variable C:Chl ratio is not needed to create a subsurface maximum in biomass. Its amplitude has the same order of magnitude, but it is shallower (35 m vs. 50 m in the standard run, Fig. 7a and 15a). Phytoplanktonic biomass is also larger

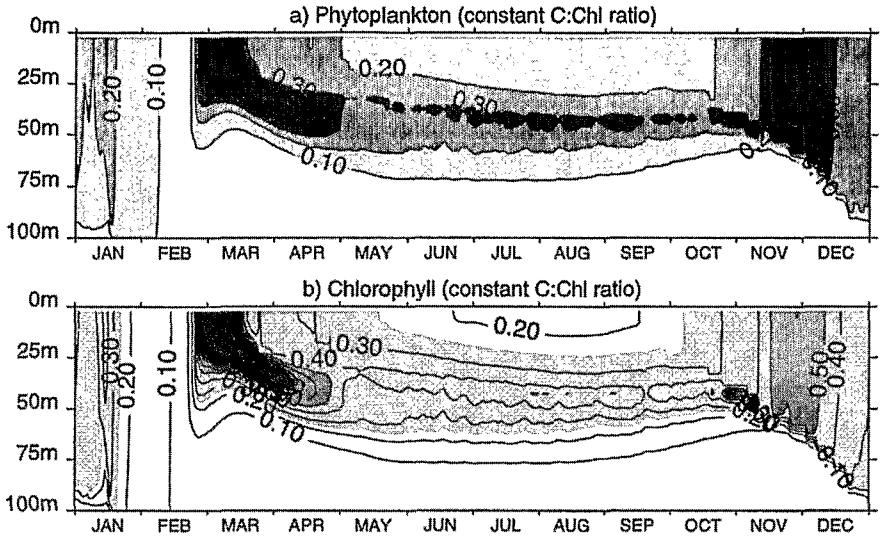

Figure 15. Annual cycle of simulated (a) phytoplankton (in mmole N m^{-3}), (b) chlorophyll (in mgChl m^{-3}) in a sensitivity experiment where the C:Chl ratio is held constant and equal to 55 mgC $(mgChl)^{-1}$.

at the sea surface, as in the standard run, the C:Chl ratio decreases with depth from surface values larger than 100 mgC $(mgChl)^{-1}$ to about 45 mgC $(mgChl)^{-1}$ at the DCM. The chlorophyll vertical gradient is larger, and the DCM a little deeper than the biomass maximum. Therefore, with a constant C:Chl ratio, the surface chlorophyll is too high by almost a factor of 3, and the DCM is too shallow and not pronounced enough. Thus it is difficult to get simultaneously reasonable surface chlorophyll concentrations, which can be validated against satellite data, and a realistic DCM, without taking into account variations of C:Chl ratio with light and nutrients. However, that does not mean that the parameterization proposed here should not be improved. Finally, with a constant C:Chl ratio of 55 mgC $(mgChl)^{-1}$, the PP is globally decreased by 16.8%, the large particle export flux by 40.8% and refractory DOM export by 9.6%. Other sensitivity studies (not shown) emphasize the delicate coupling between productivity, chlorophyll profiles and C:Chl ratio, which depends on several parameters (PUR_{max}, $R_{C:Chlmax}$, $R_{C:Chlmin}$) which are not very well constrained, and which certainly vary with phytoplanktonic populations (whereas only one type of phytoplankton is considered in BIOMELL).

b. Nitrification

Nitrification, long been neglected in the surface ocean, is now believed to be a significant nitrate source in the euphotic layer, even though it is light inhibited (Gentilhomme, 1992; Ward, 1986; Ward *et al.,* 1989). The nitrification budget predicted by the model seems impressive: 43.2% of the overall nitrate supply in the first 100 m (Fig. 12),

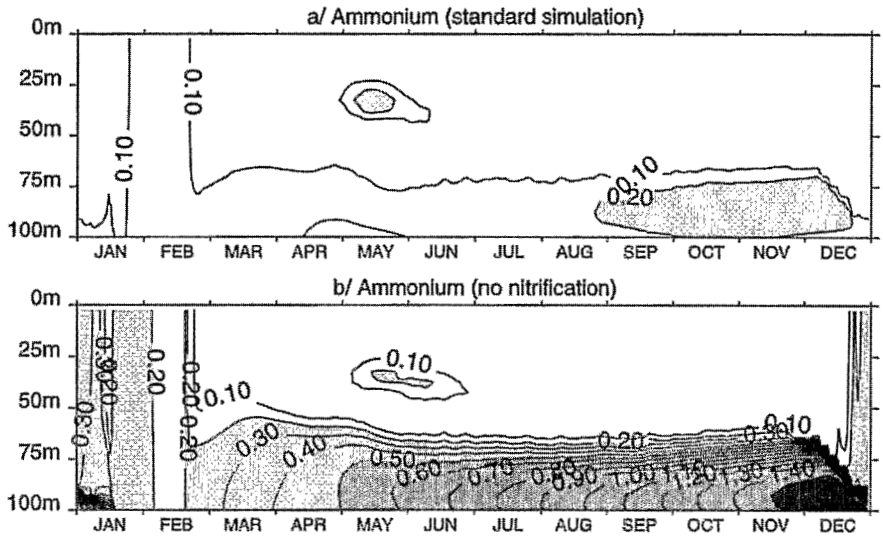

Figure 16. (a) Annual cycle of ammonium for 1991 derived by the model in the standard simulation, when nitrification is included. (b) Annual cycle of ammonium for 1991 derived in a sensitivity experiment where nitrification is not accounted for. Units are mmole N m^{-3}.

and 12.5% of the annual ammonium uptake by phytoplankton. However, there exists insufficient nitrification data to contest this assertion.

To assess the role of nitrification in BIOMELL, a sensitivity simulation is performed where nitrification is not taken into account. In this no-nitrification simulation, for consistency with the standard simulation, ammonium concentrations in winter are relaxed toward the day 40-profile of the standard simulation (similar to what is done for nitrate and DOM). Besides nitrate and ammonium (Fig. 6 and 16), all the other pools remain almost identical. The annual TP is increased (10%), resulting in a shift from regenerated nitrate-based assimilation to more efficient ammonium assimilation. Annual NP is also increased (8%), even though nitrate-based production is decreased. This increase in NP results mainly in a winter export of ammonium. With no nitrification, a highly concentrated ammonium pocket forms just under the euphotic layer, with a maximum reaching 1.6 mmoleN m^{-3} (Fig. 16b). In the Mediterranean Sea, very fiew ammonium data are available. Nevertheless, none of them reaches values larger than 0.2 mmole N m^{-3} (Gentilhomme and Slawyck, 1991; Woodward, 1994). Therefore, ammonium concentrations predicted when nitrification is taken into account (Fig. 16a) seem much more realistic. Recently, high ammonium concentrations (up to 1 mmole N m^{-3}) have been measured in the North Atlantic (BOFS data); the model, run at 20W 47N in 1989, reproduces these high values even with nitrification (not shown).

The overestimation of ammonium values when nitrification is not parameterized seems to be a general feature of biogeochemical models (Fasham *et al.*, 1993). Fasham (1995) concluded that the kinetics of ammonium assimilation are too slow, and thus decreases the

value of K_{nh4} to 0.01 mmole N m^{-3} in order to decrease the ammonium stock. In the present runs, the value used for K_{nh4} is even smaller. When the parameterization of nutrient limitation used by Fasham (1995) is taken into account in the model, nitrification is needed to obtain ammonium concentrations smaller than 2.0 mmole N m^{-3}.

Moreover, nitrate concentrations predicted by the model, when nitrification is not accounted for, are much too low below the nitracline during fall (Fig. 6, 2–3 mmole N m^{-3} instead of 3–4 mmole N m^{-3} in the standard simulation as well as in the data). In such a case, the amount of missing nitrogen in the nitrate compartment is kept in the ammonium compartment, and vertical diffusion below the nitracline is too low to sustain significant input of nitrate. Nitrate data, therefore, agree better with the simulation when nitrification is included.

Other sensitivity studies have been performed, using different parameterizations of nitrification (Michaelis-Menten kinetics, light-inhibition term). As nitrification is mainly important below the euphotic layer and when ammonium concentrations are high, the differences between these simulations and the standard one are negligible.

These simulations show that nitrification cannot be neglected. Nevertheless, not enough measurements of nitrification rate (and of its possible inhibition with light), or of ammonium concentrations are available. If it turns out that this mechanism must be considered even in the upper ocean, data are crucial: the paradigm linking annual nitrate-based production and export fluxes is no more valid.

c. Zooplankton influence

The effect of zooplankton abundance on the phytoplankton population can be either unfavorable (grazing) or favorable (excretion). The relative importance of these two processes in terms of phytoplankton growth determines the evolution of phytoplankton abundance, nutrient utilization, and, feeds back on the zooplankton growth. Microzooplankton grazing rate has been tuned to obtain satisfactory phytoplankton concentrations, particularly in the DCM where they are steady over a large period of time. A higher grazing rate (1.25 d^{-1} i.e. +25%) modifies as expected the stocks of phytoplankton and microzooplankton (respectively −15.8% and +22.4%) without modifying substantially the total production (+4.0%): microzooplankton grazing stimulates regeneration through higher excretion (+20.5%), but phytoplankton losses by grazing are also higher (+20.1%). Surprisingly, the increase of microzooplankton does not stimulate its predator. The coupling between microzooplankton and phytoplankton is faster with higher grazing rates. Therefore, the maximum in microzooplankton occurs earlier, and is not as high as in the standard run. Due to mortality and exudation, its decrease occurs earlier as well. Microzooplankton accounts for the major part (60%) of the food supply for mesozooplankton. In the sensitivity run, the mesozooplankton development occurs too late to use efficiently the microzooplankton bloom. Consequently, the particulate export is smaller

(−8.5%), and this decrease is compensated by the small DOM export increase (+4.8%). When the microzooplankton grazing rate is decreased by 25% (0.75 d^{-1}), the total export is decreased (−52.8% and −11.8% for the particulate and the DOM export respectively). The grazing rate is too small to induce a consequent microzooplankton biomass (−69%), and mesozooplankton cannot grow. Therefore, due to the non linearity of the model, with the choice of the parameters done in the standard run, modifications of the grazing rate of microzooplankton seems to always decrease the particulate flux, which is quite unexpected.

Apart from the grazing rate, zooplankton development also depends on its winter threshold value. We have tested doubled threshold values for microzooplankton and mesozooplankton separately. A higher value of Z_s^{min} allows microzooplankton to develop about one week earlier and to reach a slightly higher maximum (3%). The phytoplankton bloom is thus a couple of days shorter. The major fluxes are unchanged (by less than 1%), and the impact on mesozooplankton is too low to significantly modify the distribution of the exports. Z_l^{min} is a more sensitive parameter. With doubled Z_l^{min}, starting from higher values in spring, the mesozooplankton maximum is increased by 33%, leading to an increase of 26.3% of the particulate export. With almost the same NP, the dissolved export is decreased in consequence. Simultaneously, microzooplankton is less abundant (−9.3%), but phytoplankton abundance is quite identical (−1.6%). TP is decreased (−3.71%), as well as the total grazing pressure on phytoplankton (−15.5%). In conclusion, within these ranges, Z_s^{min} seems to control the timing of the end of the bloom while Z_l^{min} is correlated to the particulate export.

The assigned values for the microzooplankton grazing rate and the zooplankton threshold values seem satisfactory, as phytoplankton abundance and particulate export are well predicted, but are clearly interdependent as they both control the particulate export. Zooplankton mortality is another parameter which can modify significantly estimates of biomass and export fluxes. Micro and mesozooplankton data are necessary for better calibration of the model.

d. Dissolved organic matter

As already mentioned, the f_{dom_l} ratio (15%) has been tuned to reproduce the Copin-Montegut and Avril (1993) estimate of the DOC export at DyFAMed, assuming a C:N ratio of 12 for refractory DOM. A higher ratio (20%) yields to a refractory DOM compartment growth at the expense of all other variables: DOM export is enhanced by 24.6%, and large particle export lowered by 7.7%. Total production is also lower (−5.4%) because a larger part of the nitrogen is kept in the refractory DOM compartment and cannot be used for regeneration. With a smaller ratio (10%), the modifications are similar, but of opposite sign. Without refractory DOM, the large particulate export is only raised up to 4.6 gC m^{-2} y^{-1} (+17.2%), NP (i.e., total export) is thus drastically lowered. In fact, the compartments

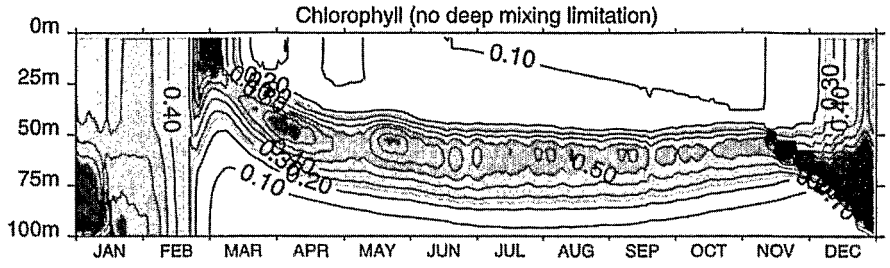

Figure 17. Annual cycle of chlorophyll derived by the model in a sensitivity experiment where the deep-mixing limitation term is not included. Units are mgChl m^{-3}.

associated with the regenerated production are greatly increased, and nitrification is almost doubled.

e. The deep mixed-layer regime growth limitation

The role of the limitation term L_M is emphasized by comparing the standard simulation to a simulation where this constraint is ignored. The differences appear clearly in the chlorophyll abundance (Fig. 7a and 17). With no limitation, winter chlorophyll concentrations are much higher than those usually observed and the spring bloom is shorter in time and less intense. This test shows that local Eulerian limitation by light, as usually defined in biogeochemical models, cannot by itself be sufficient to reproduce the low winter phytoplankton abundance in the Mediterranean Sea; Lagrangian limitation processes are to be parameterized and the chosen parameterization, in spite of its extreme simplicity, seems to be satisfactory. Moreover, the effect of winter dynamics on biology, in particular the transport of phytoplankton cells to shadow areas, appears to also be of primary importance because it preconditions the period of highest productivity, the spring bloom, and thus the export. With no mixing limiting term, phytoplankton content at the beginning of the bloom is higher, which allows production to begin sooner. Nevertheless, as zooplankton starts to grow earlier as well, its limiting effect on the bloom is more rapidly effective, and the intensity of the bloom is smaller. When photosynthesis is not explicitly limited by mixing during winter, NP, as well as export production, are increased on an annual basis by 30%.

6. Synthesis of the simulation

a. Annual balance

From the annual budget (Fig. 12), general remarks regarding the functioning of the system can be made. Grazing appears to be the most important loss term for phytoplankton. However, phytoplankton mortality is about the same order of magnitude and is therefore also of importance in the model.

Mesozooplankton is much less abundant than microzooplankton, and its grazing pressure on phytoplankton and microzooplankton is negligible compared to the other phytoplankton and microzooplankton loss terms (~5% of total losses). However, meso-

zooplankton has a crucial role in the export as it is responsible for all the large particulate export, which accounts for about 20% of the total export.

Small detritus consist of microzooplankton egestion (51%), dead phytoplankton (29%), and dead zooplankton (20%). To our knowledge, no available data can confirm these proportions. In this model, bacteria and small detritus represent the main microzooplankton food sources, before phytoplankton. Small detritus are also the main source for DOM (and therefore of DOM export), far above zooplankton excretion and phytoplankton exudation.

Bacteria is an important actor in regeneration (Fuhrman, 1992). First, they can compete with phytoplankton for ammonium assimilation. Second, bacteria assimilate DOM and recycle it almost equally towards microzooplankton growth (through grazing) and ammonium. Bacterial production based on DOM accounts for around 80% of PP. Data (Ducklow and Carlson, 1992; Ducklow *et al.,* 1995) show that this ratio is generally smaller (20–50%), although it can sometimes reach these high values (Ducklow *et al.,* 1995). BP might be overestimated by the model, which could partially explain some discrepancies between the data and the model.

Zooplankton excretion represents the other significant source of ammonium (larger than the bacteria source). This result is in good agreement with Ferrier-Pagès and Rassoulzadegan (1994) study on ammonium excretion rate in Mediterranean waters, which indicates that protozoa may account for over 50% of the nutrient recycling in these waters.

Therefore, regeneration in the model occurs through two main pathways of equal importance: a short one including phytoplankton, microzooplankton and ammonium, and another one based on bacteria assimilation of labile DOM, resulting mostly from small particle degradation. In addition to this closed system, NP fuels particulate and dissolved export and accounts for about 20% of the TP flux.

b. Turnover times

Estimation of nitrogen turnover times in each compartment presents an interesting way of describing and understanding the model behavior. This turnover time is taken as the ratio between the concentration and the net flux into or out of the compartment. Turnover times appear to be very short in the regenerated compartments (ammonium, DOM, small particles), with values of the order of one day. Kirchman *et al.* (1991) suggested that a substantial fraction of upper ocean DOC has potential turnover times of 5–100 days, which is in agreement with our estimate, summing the two DOM pools. In the primary (phytoplankton, bacteria) and secondary (microzooplankton) producer compartments, the turnover time varies between 1 day (at the surface during the bloom or at the location of the DCM during summer) and 5 days (at the surface during summer). This time is longer for mesozooplankton (5 to 30 days). These results indicate that nitrogen tends to stay longer in the higher trophic levels. They also show that turnover times are shorter where biomasses are more important.

c. Successive regimes analyses

In order to analyze each production regime, and to understand how the ecosystem switches from one regime to another, six different periods of the year, of unequal duration, are examined separately. These periods correspond either to a specific regime or to a transition period between two different regimes. In the following, values in parentheses give the mean 100 m-fluxes over these periods, and are in units of mmole N m^{-3} d^{-1}.

(1) The winter regime, corresponding to the period of deep convection (days 20 to 50). It is characterized by a deep mixed layer (more than 150 m depth), enrichment of nitrate in the mixed layer (up to about 4 mmole N m^{-3}, Fig. 6a), and low concentrations in the living compartments. Low phytoplankton production (0.78, due to winter mixing and light limitation) do not compensate mortality (0.85) and diffusive losses of phytoplankton (0.36). Therefore, phytoplankton abundance decreases over the whole period. The small detritus compartment is fed by dead phytoplankton cells, and is remineralized, through labile DOM and bacteria, to ammonium (1.85). Photosynthesis is slowed by the deep-mixing limitation, and nitrification (0.49) is much higher than nitrate uptake (0.05). As already mentioned, this period is also characterized by a large DOM export (1.99), but also an important export of bacteria (0.61) and phytoplankton (0.36) through diffusive processes.

(2) The early bloom regime, or the growth phase of phytoplankton (days 50 to 75). As soon as the water column is stabilized, production is no longer inhibited. Indeed, the shallowing of the mixed-layer from 200 m to 20 m depth in a few days has resulted in a nitrate rich mixed-layer, shallower than the euphotic layer (Fig. 5). The conditions for growth are therefore optimal. This regime is characterized by a high nitrate consumption (6.68), associated to a high *f*-ratio (0.88, neglecting nitrification). Phytoplankton keeps growing in the mixed layer, causing the shallowing of the euphotic layer. Zooplankton is still at its threshold value and does not play any role (grazing-0.22 is negligible compared to phytoplankton mortality-2.32, and particulate export-0.09 is low). As during the previous period, bacteria is the main source for ammonium (0.99, compared to 0.06 from zooplankton excretion).

(3) The late bloom regime, when primary production starts being limited (days 75 to 100). This period is characterized by the development of microzooplankton and bacteria, and decrease in mixed-layer phytoplankton content (Fig. 7a). The mixed-layer nitrate stock decreases (Fig. 6a, up to 2 mmole N m^{-3}), but is still nonlimiting. Mean fluxes suggest that microzooplankton is responsible for phytoplankton decrease, as grazing (2.88) is the trend that has the most increased from the previous period (about 13 times higher). Zooplankton use the largest part of its sources to increase its biomass, and its contribution to remineralization is still low (excretion of ammonium-0.52). Bacteria uses more ammonium (1.62) than it produces (1.57), and starts competing with phytoplankton for ammonium (ammonium-based production is 1.85).

(4) The transition regime, from bloom to oligotrophy (days 100 to 150). This period is driven by microzooplankton, which reaches its maximum biomass (Fig. 8a). Grazing

(4.44) is the first phytoplankton sink, far larger than mortality (1.48), and simultaneously zooplankton excretion is a large source of regenerated nitrogen (6.69). More generally, all the regeneration fluxes are the highest during this period (ammonium utilization by phytoplankton-5.07, by bacteria-3.18, DOM assimilation by bacteria-5.31, . . .). Most biogeochemical models produce oscillations in the phytoplankton field during that period. Here we do not get these oscillations, as long as zooplankton is allowed to graze on detritus (not shown). The very intense exchanges between microzooplankton and detritus emphasizes the role of detritus grazing in stabilizing the system (7.32 for the grazing of detritus and 9.39 for the production of fecal pellets). Such oscillations seem to be a bias inherent to the mathematical solution of the biogeochemical equations, and could only be detected using moored fluorometers. In the Sargasso Sea, Marra *et al.* (1992) have carried out this time continuous measurement and captured this transition regime, with no evidence of such oscillations. This transition period is important because it is characterized by maximum mesozooplankton growth (0.25), and therefore maximum large fecal pellet production (0.17) and substantial detritus export (0.17).

(5) The oligotrophic regime, characterized by a quasi-constant low phytoplankton biomass and the presence of a DCM (days 150–300). The system is close to steady state. The surface layer is completely nitrate depleted and phytoplankton grows at the basis of the previously set nitracline, progressively eroding it. Production is mainly regenerated (f -ratio between 0.15 and 0.3). Labile DOM assimilated by bacteria (3.55) is entirely remineralized through grazing of bacteria (3.68) and zooplankton excretion of ammonium (3.56). However, to grow on DOM, bacteria need ammonium to maintain its low C:N ratio. As in the previous regime, they compete efficiently phytoplankton to share the ammonium stock (2.13 are uptaken by bacteria, and 3.08 by phytoplankton). The mesozooplankton growth is still responsible for consequent particulate export (0.2).

(6) The late autumn-early winter regime, characterized by secondary blooms (days 300-20). Two secondary blooms occur in the 1991 simulation (Fig. 7a, mid-December and mid-January). The December bloom is associated with the progressive deepening of the mixed layer, providing new nitrate to the system, and thus breaking the previous equilibrium. As soon as the mixed layer is deeper than the euphotic layer, light limits production, causing the decrease of the bloom. In mid-January, temporarily mild weather conditions allow another secondary bloom to occur; for a few days, the surface heat forcing becomes positive (Fig. 3a), with a correlated decrease in the wind intensity (Fig. 3b). A subsequent stabilization of the mixed layer takes place (its depth varies from 100 to 40 m), initiating this secondary bloom, which is then stopped in its evolution by the occurrence of a strong wind burst on January 15. This winter bloom is consistent with observed diatom blooms that have occurred in similar conditions (Marty, 1993). It is too short to enable the development of zooplankton, and is not nutrient limited. It is thus entirely controlled by the mixed-layer depth (light limitation). This short winter bloom is responsible for an export of phytoplankton cells through mixing processes, as soon as the mixed layer deepens again. This pathway for instantaneous export have been observed in the Northeast Atlantic (Ho

and Marra, 1994). The end of these secondary blooms are thus controlled by the mixed-layer depth, in contrast with the spring bloom, which is controlled by zooplankton abundance and nutrient limitation. Other characteristics of this period are a less efficient regeneration (by about of 3 times compared to summer) and low zooplankton concentrations.

7. Summary and conclusions

In order to understand and simulate the major fluxes involved in the nutrient and carbon cycles in the ocean, a generic 10-box biogeochemical model has been developed. Following previous works (Fasham *et al.,* 1990; Prunet *et al.,* 1996), BIOMELL is based on nitrogen. It takes into account new and regenerated production, as well as the particulate and dissolved parts of the exported production. It has been validated in a rather oligotrophic region, the Northwestern Mediterranean Sea, using the dataset obtained at the DyFAMed station (DyFAMed, 1995). This region is characterized by a strong seasonal cycle, and a significant export through DOM. Coupled to a 1D mixed-layer model, and forced by the ECMWF surface fluxes, BIOMELL reproduces the annual evolution of the major stocks and fluxes for 1991.

This study has shown that several processes, although crudely represented, should be taken into account. Very low winter phytoplankton biomass can only be simulated when parameterizing Lagrangian effects of cell excursions to shadow areas by a limiting factor on growth depending on the mixed-layer depth. C:Chl dependence with light is necessary to simulate simultaneously low surface chlorophyll concentration and high pigment content in the DCM. Nitrification may be an important process, even close to the surface, which means that new production should be distinguished from nitrate based production. This process had to be taken into account in our simulation to reproduce reasonable values of ammonium. DOM export cannot be represented if an explicit semi-refractory DOM compartment is not taken into account.

Nevertheless, several important issues have not found any satisfying solution in this study. As an example, a single generic phytoplankton may be inappropriate to properly simulate production and export. Although the model is able to answer qualitatively well to the seasonal variability of the forcing, phytoplankton species follow each other according to the hydrodynamical and geochemical environment. They are characterized by different growth rates and sedimentation velocities, and probably different C:Chl ratio. Also, depending on their size, phytoplankton species have different predators, which have different grazing rates. Moreover, whether the phytoplankton considered remains in the regeneration loop (small flagellates) or is grazed by larger plankters (diatoms) and ultimately exported via large particles is a crucial question concerning the fate of organic matter, more specifically when carbon exchanges with the atmosphere are considered. Therefore, it is certainly suitable to develop models with different types of phytoplankton, all the more that zooplankton is already divided into two size classes in the BIOMELL. The

alternative choice could be to follow the ideas developed by Hurtt and Armstrong (1996) based on allometric considerations.

Making a model more complex is justified only if there is enough data to constrain its behavior and the processes involved, which brings us to a major problem concerning biogeochemical modeling. It concerns lack of data either to prescribe internal parameters or to validate the simulations, even for a model which can be considered relatively simple with regard to biological processes. At the present time, although it is believed to be crucial, very little is known about the kinetics regulating the DOM compartments. In the standard run, the partitioning between labile and refractory DOM has been tuned in order to obtain correct export fluxes, as no direct measurements were available to set that parameter. Initial conditions of zooplankton concentrations are not known, although the winter threshold value strongly constrains the intensity and the timing of the bloom, as well as the export production. The role of nitrification has only been qualitatively assessed, as there is no ammonium data at DyFAMed station. Concerning validation, the lack of microzooplankton data has already been emphasized. Finally, some basic parameters or variables are measured or evaluated in different units. For instance, phytoplankton growth rates and DOM are usually given in carbon units, whereas phytoplankton concentrations are in chlorophyll units. As the C:N ratios are not well known, and as most of the biogeochemical models use nitrogen, validation can only be qualitative, as it has been shown in the present study with DOM. This issue goes beyond validation, and puts the problem of coupling the cycles of different biogeochemical tracers, such as carbon and nitrogen.

Acknowledgments. Funding for this study was provided by French-JGOFS (Joint Global Ocean Flux Studies) program, the DRET (Direction des Recherches Etudes et Techniques), and the CNRS (Center National de la Recherche Scientifique). We are grateful to Diana Ruiz-Pino for useful discussions. We thank Jean-Claude Marty, Bernard Avril, Juan-Carlos Miquel, Jacques Chiaverini, Micheline Bianchi, France Van Wambeke and Laura Guliano for providing us the DyFAMed data. We also thank Christophe Menkes and Nicolas Metzl for helpful comments on the manuscript and Jean-Philippe Boulanger for help in the graphic outputs.

REFERENCES

Alcaraz, M. 1988. Summer zooplankton metabolism and its relation to primary production in the Western Mediterranean. Ocean. Acta, *9,* Pelagic Mediterranean Oceanography, 185–191.

Andersen, V. and P. Nival. 1988a. Modèle d'écosystème pélagique des eaux côtières de la Mer Ligure. Ocean. Acta, *9,* Pelagic Mediterranean Oceanography, 211–217.

—— 1988b. A pelagic ecosystem model simulating production and sedimentation of biogenic particles: role of salps and copepods. Mar. Ecol. Prog. Ser., *44,* 37–50.

André, J.-M. 1990. Télédétection spaciale de la couleur de la mer: algorithme d'inversion des mesures du Coastal Zone Color Scanner. Applications à l'étude de la Méditerranée occidentale. PhD, University Paris 6, France.

Antoine, D., A. Morel and J.-M. André. 1995. Algal pigment distribution and primary production in the Eastern Mediterranean as derived from coastal zone color scanner observations. J. Geophys. Res., *100,* 16193–16209.

Avril, B. 1995. Le carbone organique dissous en milieu marin. PhD, University Paris 6.

Bender, M., H. Ducklow, J. Kiddon, J. Marra and J. Martin. 1992. The carbon balance during the 1989 spring bloom in the North Atlantic Ocean, 47°N, 20°W. Deep-Sea Res., *39,* 1707–1725.

Bethoux, J.-P. 1981. Le phosphore et l'azote en mer Mediterranée, bilans et fertilité potentielle. Mar. Chem., *10,* 141–158.

—— 1989. Oxygen consumption, new production, vertical advection and environmental evolution in the Mediterranean Sea. Deep-Sea Res., *36,* 769–781.

Bianchi, M., P. Morin and P. Le Corre. 1993. Nitrification rates, nitrite and nitrate distribution in the Almeria-Oran frontal system (eastern Alboran Sea). J. Mar. Syst., *5,* 327–342.

Carlson, C. A., H. W. Ducklow and A. F. Michaels. 1994. Annual flux of dissolved organic carbon from the euphotic zone in the Northwestern Sargasso Sea. Nature, *371,* 405–408.

Cho, B. C. and F. Azam. 1990. Biogeochemical significance of bacterial biomass in the ocean's euphotic zone. Mar. Ecol. Prog. Ser., *63,* 253–259.

Claustre, H. 1994. The trophic status of various oceanic provinces as revealed by phytoplankton pigment signatures. Limnol. Oceanogr., *39,* 1206–1210.

Cloern, J. E., C. Grenz and L. Vidergar-Lucas. 1995. An empirical model of the phytoplankton chlorophyll:carbon ratio—the conversion factor between productivity and growth rate. Limnol. Oceanogr., *40,* 1313–1321.

Copin-Montegut, G. and B. Avril. 1993. Vertical distribution and temporal variation on dissolved organic carbon in the Northwestern Mediterranean Sea. Deep-Sea Res., *40,* 1963–1972.

Doney, S. C., D. M. Glover and R. G. Najjar. 1996. A new coupled one dimensional biological-physical model for the upper ocean: applications to the JGOFS Bermuda Atlantic Time series Study (BATS) site. Deep-Sea Res., *43,* 591–624.

Drange, H. 1994. An isopycnic coordinate carbon cycle model for the North Atlantic; and the possibility of disposing of fossil fuel CO2 in the ocean. PhD, University of Bergen, Norway.

Ducklow, H. W. and C. A. Carlson. 1992. Oceanic bacterial production, *in* Advances in Microbial Ecology, P. P. K. C. Marshall, New-York, 113–181.

Ducklow, H. W., C. A. Carlson, N. R. Bates, A. H. Knap and A. F. Michaels. 1995. Dissolved organic carbon as a component of the biological pump in the North Atlantic Ocean. Phil. Trans. R. Soc. Lond, *348,* 161–167.

Dugdale, R. C. and J. J. Goering. 1967. Uptake of new and regenerated forms of nitrogen in primary productivity. Limnol. Oceanogr., *12,* 196–206.

DYFAMED-JGOFS France. 1995. Recueil de données (Janvier 1991–Decembre 1993).

Eppley, R. W., C. Garside, E. H. Renger and E. Orellana. 1990. Variability of nitrate concentrations in nitrogen-depleted subtropical surface waters. Mar. Biol., *107,* 53–60.

Eppley, R. W. and R. W. Koeve. 1990. Nitrate use by plankton in the eastern subtropical North Atlantic, March–April 1989. Limnol. Oceanogr., *35,* 1781–1788.

Eppley, R. W. and B. J. Peterson. 1979. Particulate organic matter flux and planktonic new production in the deep ocean. Nature, *282,* 57–70.

Fasham, M. J. R. 1995. Variations in the seasonal cycle of biological production in subarctic oceans: a model sensitivity analysis. Deep-Sea Res., *42,* 1111–1149.

Fasham, M. J. R., H. W. Ducklow and S. M. McKelvie. 1990. A nitrogen-based model of plankton dynamics in the oceanic mixed-layer. J. Mar. Res., *48,* 591–639.

Fasham, M. J. R., J. L. Sarmiento, R. D. Slater, H. W. Ducklow and R. Williams. 1993. Ecosystem behavior at Bermuda station "S" and ocean weather station "India": a general circulation model and observational analysis. Global Biogeo. Cycles, *7,* 379–415.

Ferrier-Pagès, C. and F. Rassoulzadegan. 1994. N remineralization in planktonic protozoa. Limnol. Oceanogr., *39,* 411–419.

Fowler, S. W., L. F. Small and J. La Rosa. 1991. Seasonal particulate carbon flux in the coastal Northwestern Mediterranean Sea, and the role of zooplankton fecal matter. Ocean. Acta, *14,* 77–85.

Frost, B. W. 1987. Grazing control of phytoplankton in the open subarctic Pacific Ocean: a model assessing the role of mesozooplancton, particularly the large calanoid copepods Neocalanus spp. Mar. Ecol. Prog. Ser., *39,* 49–68.

Fuhrman, J. 1992. Bacterioplankton roles in cycling of organic matter: the microbial food web, *in* Primary Productivity and Biogeochemical Cycles in the Sea, P. G. Falkowski and A. D. Woodhead, Plenum Press, New-York, 361–383.

Gascard, J. C. 1978. Mediterranean deep water formation, baroclinic instability and oceanic eddies. Ocean. Acta, *1,* 315–330.

Gaspar, P., Y. Gregories and J. M. Lefevre. 1990. A simple eddy kinetic energy model for simulations of the oceanic vertical mixing: tests at station papa and long term upper ocean study site. J. Geophys. Res., *95,* 16179–16193.

Gentilhomme, V. 1992. Quantification des flux d'absorption et de regeneration de l'azote mineral (nitrate, nitrite et ammonium) et organique (urée) dans la couche euphotique des océans oligotrophes. PhD, University of Aix-Marseille II, France.

Gentilhomme, V. and G. Slawyk. 1991. Dosage de l'ammonium et de l'urée dans la couche euphotique, In Production pélagique de la Méditerranée sub occidentale, Campagne Mediprod VI, campagnes Océanographiques Francaises, *16,* 133–138.

Gostan, J. and P. Nival. 1963. Distribution hivernale des caractéristiques hydrologiques en mer Ligure et estimation de l'abondance du phytoplancton par la methode des pigments. C. R. Acad. Sc. Paris, *257,* 2872–2875.

Gran, H. and T. Braarud. 1935. A quantitative study of phytoplankton in the Bay of Fundy in the Gulf of Maine. J. Biol. Board. Canada, *I (5),* 279–467.

Harrison, W. G., L. R. Harris and B. D. Irwin. 1996. The kinetics of nitrogen utilization in the oceanic mixed-layer: nitrate and ammonium interactions at nanomolar concentrations. Limnol. Oceanogr., *41,* 16–32.

Ho, C. and J. Marra. 1994. Early-spring export of phytoplankton production in the Northeast Atlantic Ocean. Mar. Ecol. Prog. Ser., *114,* 197–202.

Houghton, J. T., G. J. Jenkins and J. J. Ephraums. 1990. Climate Change: the IPCC Scientific Assessment, WMO, UNEP.

Hurtt, G. C. and R. A. Armstrong. 1996. A pelagic ecosystem model calibrated with BATS data. Deep-Sea Res., *43,* 653–683.

Jacques, G. 1988. Flux de carbone en milieu pélagique de Méditerranée occidentale lors de la floraison printanière. Ocean. Acta, *9,* Pelagic Mediterranean Oceanography, 143–148.

Jacques, G., M. Minas, J. Neveux, P. Nival and G. Slawyk. 1976. Conditions estivales dans la divergence de Méditerranée Nord-Occidentale. III. Phytoplancton. Ann. Inst. Oceanogr., *52,* 141–152.

Kirchman, D. L., Y. Susuki, C. Garside and H. W. Ducklow. 1991. Bacterial oxidation of dissolved organic carbon in the North Atlantic cean during the spring bloom. Nature, *352,* 612–614.

Krstulovic, N., T. Pucher-Petkovic and M. Solic. 1995. The relation between bacterioplankton and phytoplankton production in the mid Adriatic Sea. Aquat. Microb. Ecol., *9,* 41–45.

Lawson, L. M., E. E. Hofmann and Y. H. Spitz. 1996. Time series sampling and data assimilation in a simple marine ecosystem model. Deep-Sea Res., *43,* 625–651.

Lefèvre, D., M. Denis, C. Lambert and J.-C. Miquel. 1996. Is DOC the main source of organic matter remineralization in the ocean water column? J. Mar. Syst., *7,* 281–291.

Lévy, M. 1996. Modélisation des cycles biogéochimiques en Méditerranée nord-occidentale: variabilité mésoéchelle et cycle saisonnier. PhD, Paris 6.

Longhurst, A. R. and W. G. Harrison. 1989. The biological pump: profiles of plankton production and consumption in the upper ocean. Prog. Oceanogr., *22,* 47–123.

Marra, J., T. Dickey, W. S. Chamberlin, C. Ho, T. Granata, D. A. Kiefer, C. Langdon, R. Smith, R. Bidigare and M. Hamilton. 1992. Estimation of seasonal primary production from moored optical sensors in the Sargasso Sea. J. Geophys. Res., *97,* 7399–7412.

Marty, J.-C. 1993. Opération DYFAMED, rapport d'activité pour 1993 et programme pour 1994, programme France/JGOFS.

Marty, J.-C., B. Avril, G. Copin-Montegut and J.-C. Miquel. 1994a. Importance of the dissolved pathway in the vertical flux of carbon in the Ligurian Sea, n°3, Le courrier de JGOFS-France.

Marty, J.-C., E. Nicolas, J. C. Miquel and S. W. Fowler. 1994b. Particulate fluxes of organic compounds and their relationship to zooplancton fecal pellets in the Northwestern Mediterranean Sea. Mar. Chem., *46,* 387–405.

McGillicuddy, D. J., J. J. McCarthy and A. R. Robinson. 1995. Coupled physical and biological modeling of the spring bloom in the North Atlantic (I): model formulation and one dimensional bloom processes. Deep-Sea Res., *42,* 1313–1357.

Medoc group. 1970. Observation of formation of deep water in the Mediterranean Sea, 1969. Nature, *227,* 1037–1040.

Millot, C. 1987. Circulation in the Western Mediterranean Sea. Ocean. Acta, *9,* Pelagic Mediterranean Oceanography, 143–149.

Minas, H. J. 1970. La distribution de l'oxygène en relation avec la production primaire en Méditerranée nord-occidentale. Mar. Biol., *7,* 181–204.

Minas, H. J. and M.-C. Bonin. 1988. Oxygénation physique et biologique de la Méditerranée nord-occidentale en hiver et au printemps. Ocean. Acta, *9,* Pelagic Mediterranean Oceanography, 123–131.

Minas, H. J. and L. A. Codispoti. 1993. Estimation of primary production by observation of changes in the mesoscale nitrate field. ICES Mar. Sci. Symp., *197,* 215–235.

Minas, H. J., M. Minas, B. Coste, J. Gostan, P. Nival and M. C. Bonin. 1988. Production de base et de recyclage; une revue de la problèmatique en Méditerranée Nord-Occidentale. Ocean. Acta, *9,* 155–162.

Miquel, J.-C., S. W. Fowler and J. La Rosa. 1993. Vertical particle fluxes in the Ligurian Sea. Ann. Inst. Oceanogr., *69,* 107–110.

Miquel, J.-C., S. W. Flower, J. La Rosa and P. Buat-Menard. 1994. Dynamics of the downward flux of particles and carbon in the open Northwestern Mediterranean Sea. Deep-Sea Res., *41,* 243–262.

Morel, A. 1988. Optical modeling of the upper ocean in relation to its biogenous matter content (case I waters). J. Geophys. Res., *93,* 10749–10768.

Morel, A. 1991. Light and marine photosynthesis: a spectral model with geochemical and climatological implications. Prog. Oceanogr., *26,* 263–306.

Morel, A. and J.-M. André. 1991. Pigment distribution and primary production in the western Medterranean, as derived and modeled from coastal zone color scanner observations. J. Geophys. Res., *96,* 12685–12698.

Nival, P., S. Nival and A. Thiriot. 1975. Influence des conditions hivernales sur les productions phyto-et zooplanctoniques en Méditerranée nord-occidentale. V: Biomasse et production zooplanctonique-relations phyto-zooplancton. Mar. Biol., *31,* 249–270.

Pollehne, F., B. Klein and B. Zeitzschel, 1993. Low light adaptation and export production in the deep chlorophyll maximum layer in the Northern Indian Ocean. Deep-Sea Res., *40,* 737–752.

Prunet, P., J.-F. Minster, D. Ruiz Pino and I. Dadou. 1996. Assimilation of surface data in a one-dimensional physical biogeochemical model of the surface ocean. 1. Method and preliminary results. Glob. Biogeochem. Cycl., *10,* 111–138.

Raimbault, P., M. Rodier and I. Taupier-Letage. 1988. Size fraction of phytoplankton in the Ligurian Sea and the Algerian Basin (Mediterranean Sea): size distribution versus total concentration. Mar. Microbial Food Webs, *3,* 1–7.

Razouls, C. and J. H. M. Kouwenberg. 1993. Spatial distribution and seasonal variation of mesozooplankton biomass in the Gulf of Lions (Northwestern Mediterranean). Ocean. Acta, *16,* 393–401.

Riley, G. A. 1942. The relationship of vertical turbulence and spring diatom flowerings. J. Mar. Res., *5,* 67–87.

Sarmiento, J. L., R. D. Slater, M. J. R. Fasham, J. R. Ducklow, J. R. Toggweiler and G. T. Evans. 1993. A seasonal three-dimensional ecosystem model of nitrogen cycling in the North Atlantic euphotic zone. Glob. Biogeochem. Cycl., *7,* 417–450.

Siegenthaler, U. and J. L. Sarmiento. 1993. Atmospheric carbon dioxide and the ocean. Nature, *365,* 119–125.

Simonot, J.-Y. 1988. Thermodynamic-biological-optical coupling in the oceanic mixed-layer. J. Geophys. Res., *93,* 8193–8202.

Small, L. F., G. A. Knauer and M. D. Tuel. 1987. The role of sinking fecal pellets in stratified euphotic zones. Deep-Sea Res., *34,* 1705–1712.

Sverdrup, H. U. 1953. On conditions for the vernal blooming of phytoplankton. J. Cons. Int. Expor. Mer., *18,* 287–295.

Takahashi, T., W. S. Broecker and S. Langer. 1985. Redfield ratio based on chemical data from isopycnal surfaces. J. Geophys. Res., *90,* 6907–6924.

Ward, B. B. 1986. Nitrogen transformations in the Southern California Bight. Deep-Sea Res., *34,* 785–805.

Ward, B. B., K. A. Kilpatrick, E. H. Renger and R. W. Eppley. 1989. Biological nitrogen cycling in the nitracline. Limnol. Oceanogr., *34,* 493–513.

Woods, J. D. and R. Onken. 1982. Diurnal variation and primary production in the ocean—preliminary results of a Lagrangian ensemble model. J. Plankton Res., *4,* 735–756.

Woodward, E. M. S. 1994. Nanomolar ammonia concentrations in the western Mediterranean, *in* Water Pollution Research, report 32, J. M. Martin and H. Barth, eds., 87–96.

Yamazaki, H. and D. Kamykowski. 1991. The vertical trajectories of motile phytoplankton in a wind-driven water column. Deep-Sea Res., *38,* 219–241.

Received: *29 January, 1997;* revised: *30 September, 1997.*